2012

Phenotyping C.elegans and Neuronal Cells in Microengineered Devices

Roy James Lycke
Iowa State University

Phenotyping *C.elegans* and neuronal cells in microengineered devices

by

Roy James Lycke

A thesis submitted to the graduate faculty in partial fulfillment of the requirements for the degree of

MASTER OF SCIENCE

Major: Computer Engineering

Program of study committee:
Santosh Pandey, Major Professor
Timothy Bigelow
Phillip Jones

Iowa State University
Ames, Iowa
2012

Table of Contents

List of Figures

List of Tables

.

Acknowledgment

I am grateful to those who helped me get to where I am today. Chief among these people is Dr. Santosh Pandey. It was by his guidance that I pursued a Masters at Iowa State, achieved an NSF student fellowship, and found the next university that I will attend in my academic career. Besides, my research perspective has benefitted tremendously from Dr. Donald Sakaguchi and Dr. Richard Martin. I am extremely grateful to Dr. Sakaguchi for providing access to his laboratory and training me countless hours on cell culturing.

I must also thank the members of my POS committee. I was part of an IEEE Honors Society, Eta Kappa Nu, which was mentored very well by Dr. Timothy Bigelow. Dr. Phillip Jones always forced me to think critically and taught me to design and build systems beyond my wildest expectations. From my lab group, I must give deserving thanks to Archana Parashar. She has been a fount of knowledge and giver of guidance, my entire time as a graduate student. So many times she corrected my mistakes and improved my methods, improving how I conduct myself in all research and giving me keen analytical eye. I am equally thankful to our group's past students including John Carr and Baozhen Chen.

In addition to all those in my academic life, I want to acknowledge my father, Steve Lycke. Like many parents, he supported me and drove me onward, always giving his all so that I could succeed. But in addition to all this, he taught me to question everything. He showed me how to think, to seek truth, and cultivate my understanding of the world. As a thankful son, I can tell him, "You've succeeded because you've raised me into a man who will seek to enrich the world through new discoveries and the truth."

Lastly, I give thanks to God. It is through him that all I have I have received and by his grace that my soul is calm in turbulent times and joyful in good times. I will continue to serve and strive to better the world in his service.

Abstract

Phenotype denotes the observable traits or behaviors of any living subject such as cells, animals, and humans. In the post-genomics era, the next major challenge in the biological community is establishing the link between genotype and observed phenotype. Even though phenotypic characterization of higher mammals is complicated, it is possible to quantify the phenotype of live cells and model organisms with relative accuracy. In this respect, engineering platforms are being created with controlled microenvironments and ease of manipulation to quantify visible behavioral differences. Such platforms are especially developed to enable increased experimental throughput, data reproducibility, device robustness, and system versatility. With these broad goals, this thesis focuses on two technology platforms families that we built in our research group. The first platform family is microfluidic systems with real-time imaging to characterize the behavior of *Caenorhabditis elegans* microorganisms under chemical, electrical or mechanical stimulation. The second platform family is microelectronic/microfluidic assays to quantify the degree of cell migration among different cell populations. For each of the two platforms families, the process of device development, system assembly, software interface, and experimental results are presented. The results demonstrate the advantage of using microscale technologies, particularly high spatial and temporal resolution, for studying phenotype and lead our discussion to future technological considerations for successful adoption in biological laboratories. Lastly, this thesis also emphasizes the need for sustained collaborations between engineers and biologists for proper problem identification and proposed solutions.

Chapter 1

Distinguishable Modes of *C.elegans* Paralysis upon Exposure to Different Anthelmintic Drugs

1.1 Introduction

C.elegans has established itself as a model organism in the fields of genetics, molecular biology, and neurophysiology. The key reasons that contribute to its wide acceptability in the biological community are its matured genetics, short lifespan, conserved genes through generations, and relative ease of culture. *C.elegans* has also been used in electrophysiological studies geared towards the discovery of new drugs and the understanding of their molecular modes of actions [1-3]. Traditionally, inhibition assays are used to assess the survivability of worms in a certain drug or to quantify the dose-related effects of the drug on worm survivability [4-7]. Besides measuring the percentage of worms surviving a given drug concentration, it is difficult to measure any other key parameters in the inhibition assays because of the macroscopic platform that is incompatible for real-time imaging. In this regards, we propose to develop a two-dimensional microfluidic platform where we can observe worm behavior at real-time and discover differences in worm motility under different drug environments.

1.1.1 Objectives

The objective of this project is to build a microfluidic device where *C. elegans* will be exposed to four drug solutions, their behavior recorded at real-time, and their motility parameters identified to characterize the effects of drugs on the worm behavior.

1.2 Methods & Procedures

1.2.1 Device Fabrication

The microfluidic device is fabricated using standard soft lithography. The device design is drawn in AutoCAD and sent out to an outside vendor (Fineline Imaging, Colorado Springs, CO) for printing the black-and-white masks. A UV-sensitive polymer, SU-8 (Microchem Corpation, Newton, MA), is spin-coated on a clean, 3-inch silicon wafer to create an 80 μm thick layer. The SU-8 is patterned with the features on the physical mask and developed. Later, PDMS polymer (Sylgar 184 Silicone Elastomer Kit, Dow Corning Corporation, Midland, MI) is poured on the SU-8 master and allowed to dry in a low-pressure chamber. The dried PDMS is peeled off the SU-8 master, punched with holes for the fluidic ports, and irreversibly bonded to a glass slide.

1.2.2 Experimental Setup

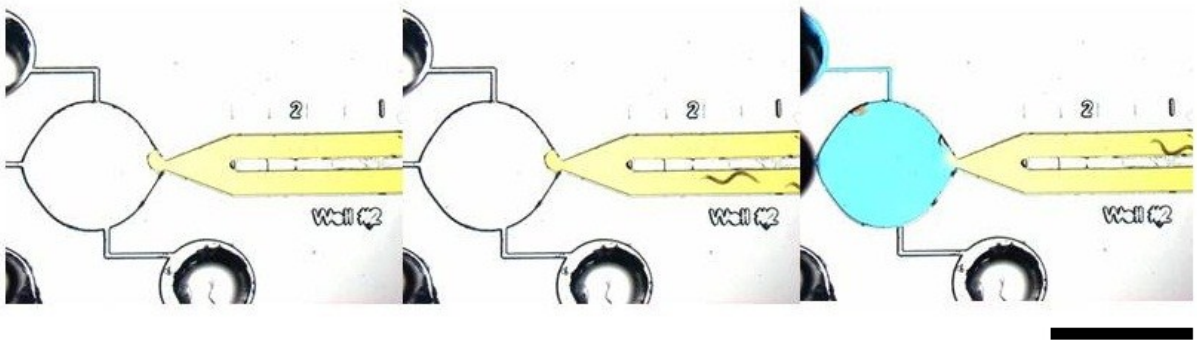

Figure 1.1: Photographs of each step in the loading procedure of the microfluidic device. Yellow media represents 0.8% agarose gel and blue media represents drug solution. Scale bar is 2 mm.

The device is filled in a two-step procedure as shown in Figure 1.1. In the first step, 0.8% agarose gel is loaded in a syringe and slowly filled into the straight microchannel. The filling is stopped when the forward profile of the agar reaches the tapered mouth of the microchannel. Single L4-stage worms are picked from the culture plate with a sterilized wire and dropped at the input port. After a wait time of around 5-7 minutes, the worms enter the microchannel and migrate towards its tapered mouth. As the drug well is filled with air, the worms are restricted in the microchannel. In the second step, a mixture of 0.8% agarose gel and the drug solution under test is prepared and filled into the drug well through the side port. Two platinum electrodes are inserted in the agarose gel, one in the input port and one in the side port, and connected to a DC voltage supply. An electric field is applied (~ 5 Volts/cm) between the two electrodes that attract the worms to the drug well and enter.

A Leica stereozoom microscope is connected with a high-speed QImaging Camera for real-time recording of worm behavior in the drug well. In our present configuration, we could observe four drug wells (of four individual devices) within the field of view, but only one drug well was imaged at high resolution. The camera is programmed to record images every one second for 40 minutes, which are later sequenced into a single .avi video file for further data analysis.

1.2.3 Analysis Techniques

All experiments were conducted multiple times (N > = 4), each with a certain number of worms (n >= 5). The recorded videos were saved in a file folder. Before every drug test, control tests were run in agar or DMSO to ensure the proper health of worm samples and functioning of the microfluidic device. To minimize any human bias during data analysis, a team of two individuals performed the following procedure: First person (A.P) prepared the drug solution, second person (R.L.) ran the microfluidic experiments (without knowing the drug under test), first person renamed the individual video files before data analysis, second person performed the data analysis, and finally all the extracted data was assembled by the first person. Later, some random tests were conducted by the two individuals using single blind analysis to verify the final data sets. Statistical analysis was performed using the GraphPad Prism software.

1.3 Results

We previously reported the dose response characteristics (i.e. percentage of worms responsive to electric field) of *C.elegans* upon exposure to levamisole in the developed microfluidic device. Similar dose response characteristics were measured for three other drugs: tribendimidine, pyrantel, and methyridine. To test the mechanism of paralysis, we chose a critical drug concentration where the percentage of worms responsive to electric fields was approximately 25%, see figure 1.2. At this concentration we previously observed worms paralyzing and showing unique behaviors whereas at higher drug concentrations (lower percentage of worms responsive) worms paralyzed too quickly to show unique behaviors and at low drug concentrations (higher percentage of worms responsive) too few worms paralyzed for definite characteristics to be observed.

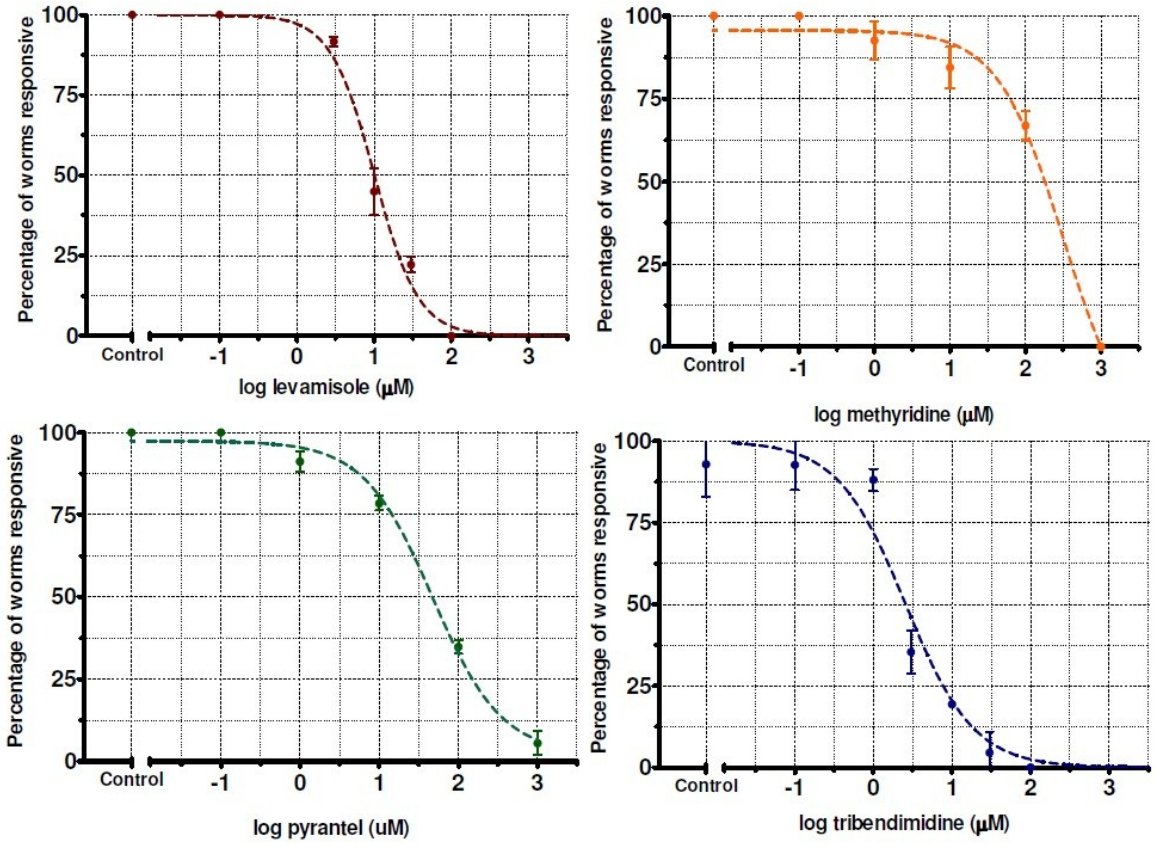

Figure 1.2: Drug response curves showing percentage of worms responsive after exposure to different concentrations of the drugs levamisole, methyridine, pyrantel, and tribendimidine.

Sample videos of worm locomotion in the drug well filled with four individual drugs are attached as Supplementary files. Upon reviewing the videos, some differences in worm locomotion are obvious to the human eye. For instance, worms tend to exhibit a 'swimming' behavior in methyridine while demonstrating the usual sinusoidal 'crawling' behavior in the other three drugs. Furthermore the videos reveal some fundamental differences in the nature of body movements before a worm paralysis in the four drug cases. To accurately quantify the modes of *C.elegans* paralysis in different drugs, we devised a list of movement parameters that can be measured from our recorded videos.

Our initial tests suggested a marked difference in the rate of curling actions exhibited by the *C.elegans*. Figure 1.3 shows a series of images to describe the progression of a curl exhibited by a sample *C.elegans* in the microfluidic drug well. For our analysis, a curl is defined when a worm's head touches or overlaps its tail. Using this definition, we revisited the recorded videos and manually counted the total number of curls exhibited by every active worm (i.e. worm that has not yet paralyzed) in the video. Thereafter, the number of curls per second was calculated by dividing the total number of curls by the total active time for every worm. The number of curls per second is plotted for all the four anthelmintic drugs. The data suggests that number of curls per second is significantly higher in levamisole, tribendimidine and pyrantel than in methyridine, DMSO and agar.

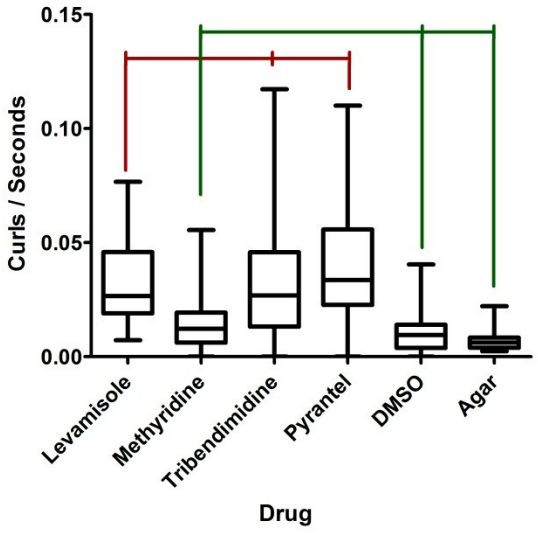

Figure 1.3: The curling rate observed for *C.elegans* in different drug solutions. The two groups labeled by the green and red bars show significant difference for each drug to the other group (opposing color) but no difference to drugs within the same group.

Besides the prominent curling action upon exposure to drugs, an active worm also changed the nature in which it carried their entire body in the drug well. Based on our observations, we generalize their nature of body displacement into crawling, curling, and flailing. Crawling is the undulatory, sinusoidal movement of the worm that results in forward or backward locomotion. Curling, as defined earlier, is resulted when the worm's head touches or overlaps its tail. On several occasions, especially upon drug exposure, a worm appears to 'flail' or oscillate its body in half waves about a fixed location. During an experiment, an active worm may exhibit any of the abovementioned three modes of motion (i.e. crawling, curling, and flailing). We manually counted the transitions made by an active worm among the 8 different positions which describe the full range of a *C.elegans*' motion within these 3 modes of motion upon exposure to the four drugs. The number of mode transitions was counted within three time windows of worm entry into the drug well: 30 seconds, 1 minute, and 2 minutes. The data is plotted in Figure 1.4. The number of mode transitions is significantly higher in methyridine and pyrantel compared to the number of mode transitions in levamisole and tribendimidine. Interestingly, worms exhibited more frequent flailing motion in methyridine compared to in other three drugs.

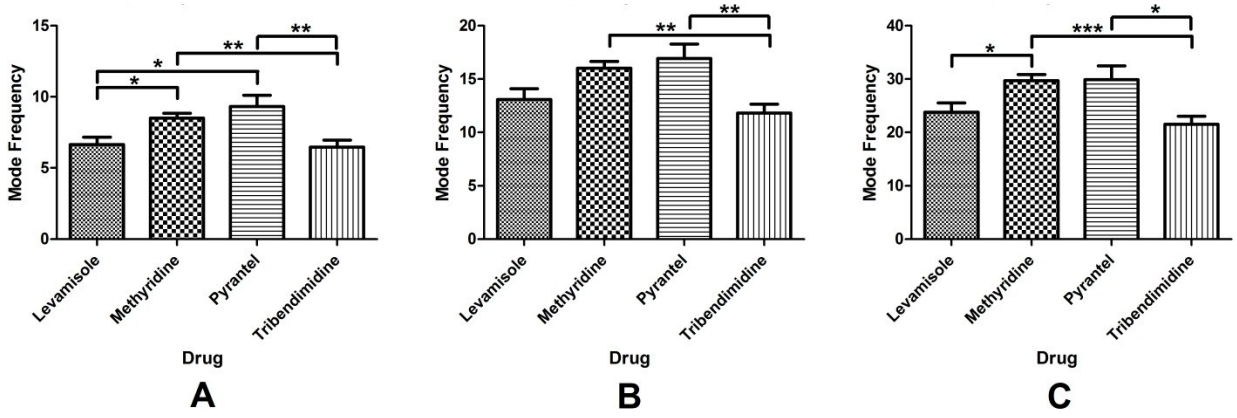

Figure 1.4: Observed mode frequency for *C.elegans* in different drug solutions for A) 30 seconds, B) 1 minutes, and C) 2 minutes. The mode frequency is calculated based on the transitions from one position to another, thus giving an accurate representation of the worm's overall activity level regardless of forward motion.

As a worm enters the drug well, it shows immobilization patterns that can be grouped into three categories: active, temporarily immobilized, permanently immobilized. Based on our definition, a worm is considered active if its body is displaced from its original location within a given timeframe (15 seconds); after 15 seconds the worm is considered immobilized. A worm is permanently immobilized if its entire body remains stationary for at least 600 seconds. On

several occasions, an active worm appears to have 'spasm-like events' before becoming permanently immobilized. In the case of temporary immobilization a worm is immobile for at least 15 seconds or longer but returns to activity before 600 seconds and is never immobilized for 600 seconds during the entire recording. Figure 1.5 shows an illustration of a worm experiencing multiple temporary immobilizations within the microfluidic device. We used our previously designed worm tracking program to locate the body centroid of individual worms in the drug well over the length of the recorded video. The tracks of a sample worm are plotted this Figure, showing the time periods when the worm is active, temporarily immobilized or permanently immobilized. During the active period, the worm moves freely and its track appears roughly as a straight line. During the temporarily immobilized period, the worm is motionless and its track appears as a small circle or dot; this is the same as would be seen for a permanent immobilization, except for at least 600 seconds.

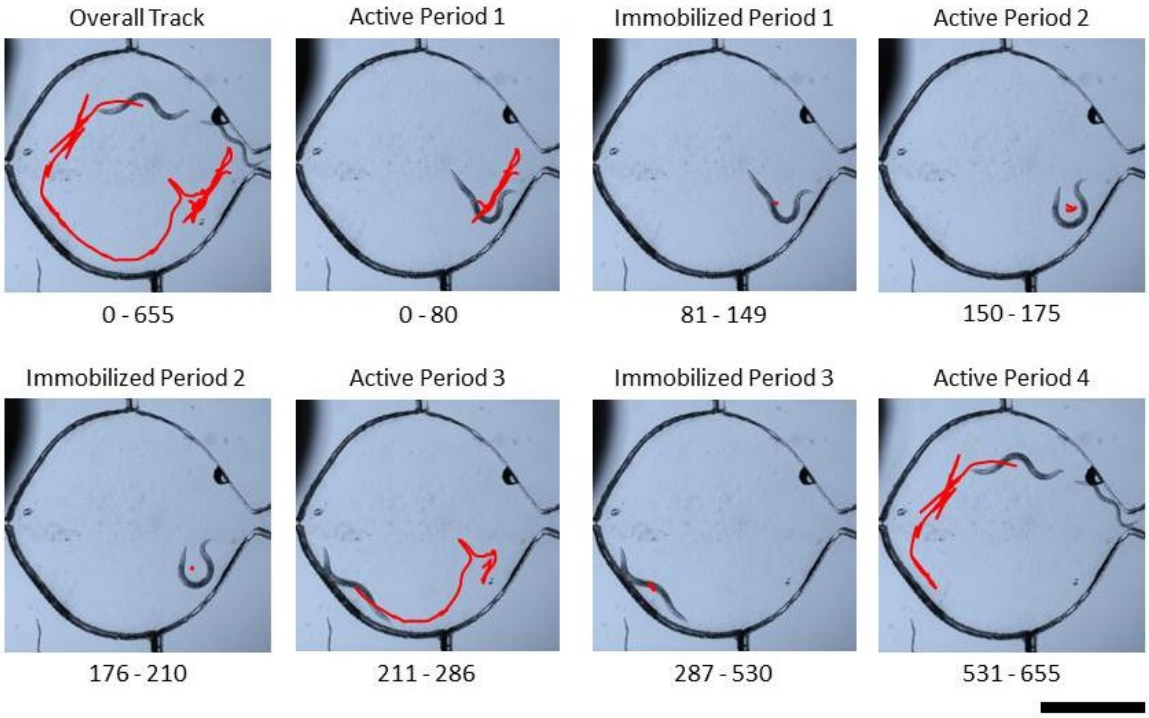

Figure 1.5: Track of a *C.elegans* (in red) exposed to levamisole with active and immobilized periods separated and tagged by frame count which corresponds to seconds after entering the drug well. The worm above was only temporarily immobilized in this trial. Scale bar is 1 mm.

Figure 1.6 plots the percentage of worms that were active, temporarily immobilized, or permanently immobilized at the end of their 40 minutes exposure to the four drugs. As shown, all worms appear active in agarose medium. The percentage of worms permanently immobilized in pyrantel and tribendimidine is significantly higher than those permanently immobilized in methyridine and DMSO. In levamisole, the percentage of worms permanently immobilized is higher than in methyridine but lower than that pyrantel or tribendimidine.

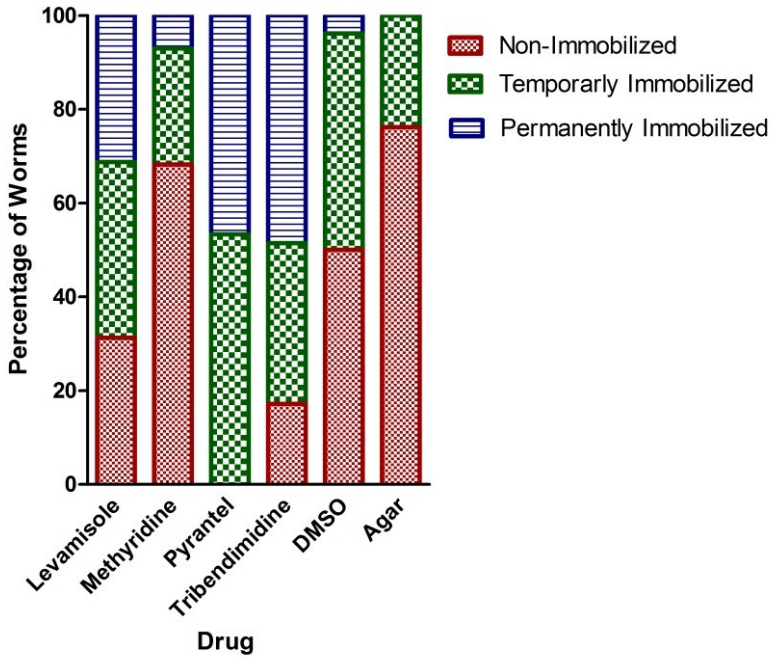

Figure 1.6: Bar-chart describing the percentage of worms that are never paralyzed, temporarily paralyzed, or permanently paralyzed during their 40 minute exposure to drug for each drug (levamisole, methyridine, pyrantel, tribendimidine, DMSO, and agar).

As mentioned before, an active worm entering the drug well may exhibit several cycles of temporary immobilization before succumbing to the drug and permanently immobilizing. From the recorded videos, we manually counted the number of times a worm enters the active phase or the temporarily immobilization phase. Figure 7a and 7b plot the percentage of worms as a function of the number of active cycles and immobilization cycles they demonstrate in the drug well, respectively. All the plots start at 100% in the first active cycle as all worms entering the drug well are active. In the control tests with agarose, 20% of the worms appear temporarily immobilized before becoming active again (i.e. in the second active cycle). No worm entered the second immobilization cycle in agarose. Compared to the other three drugs, we see fewer

immobilization cycles in tribendimidine because most worms fail to recuperate and enter the active cycle after a small number of immobilization cycles. In methyridine and DMSO, the effects on active and immobilization cycles are similar. Similarly, the effects of pyantel and levamisole are shown as an increased number of active and immobilization cycles.

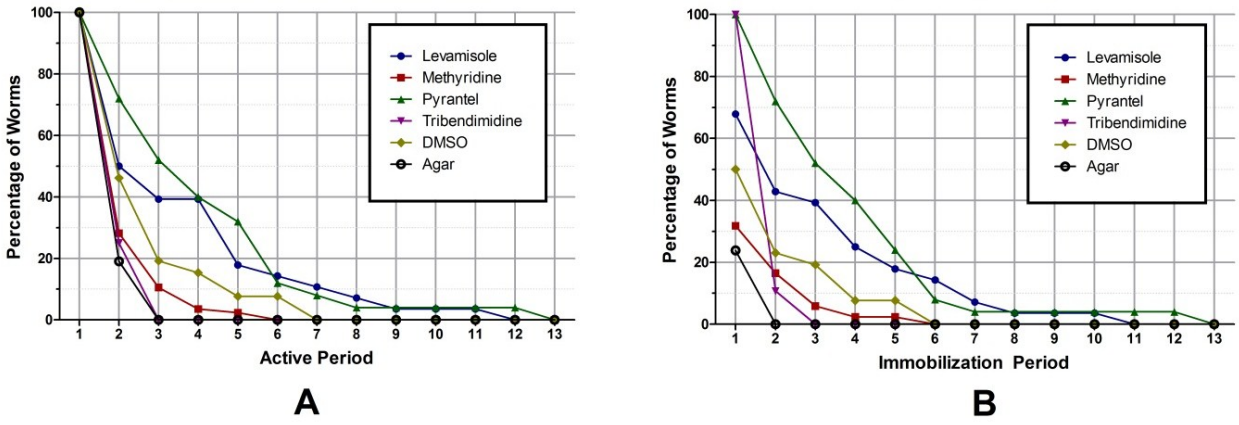

Figure 1.7: The percentages of all *C.elegans* entering the drug well that reached progressive cycle of (A) activity or (B) immobilization. All drug show 100% worms active for the first active period because this corresponds to the period when the worms first entered the drug well.

The time period a worm stays in each active or immobilization cycle also varies upon exposure to the four drugs. Figure 1.8 and 1.9 plot the time spent in the active and immobilization cycles, respectively. In general, the duration spent in each active or immobilization cycle decreases with the progression of the drug exposure. In tribendimidine, the time spent in the initial immobilization cycles is greater than that in the later cycles.

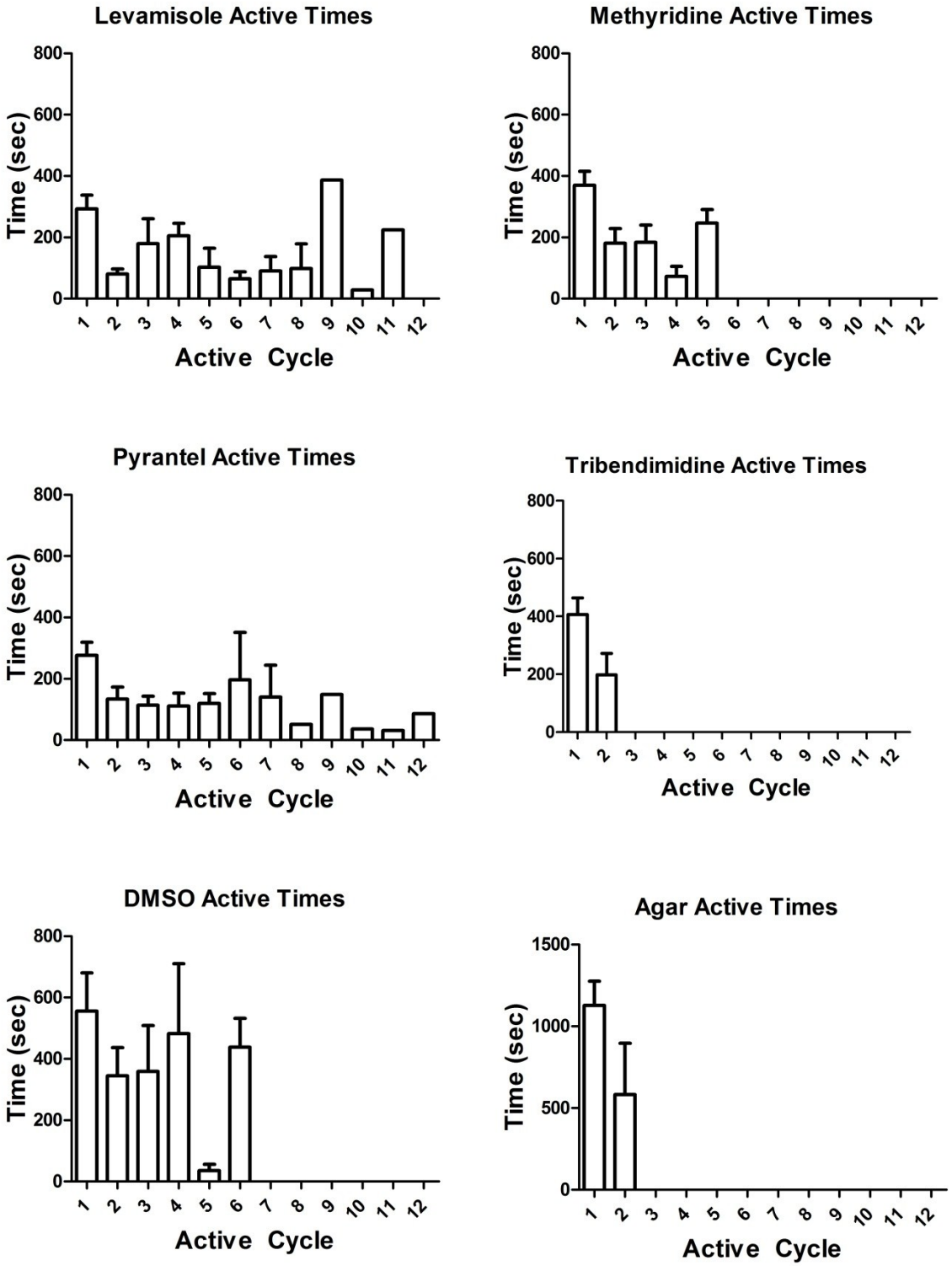

Figure 1.8: The observed median active times for each active period when *C.elegans* were exposed to a variety of drug conditions (levamisole, methyridine, pyrantel, tribendimidine, DMSO, and agar). All graphs except the agar active times graph have the same axis units.

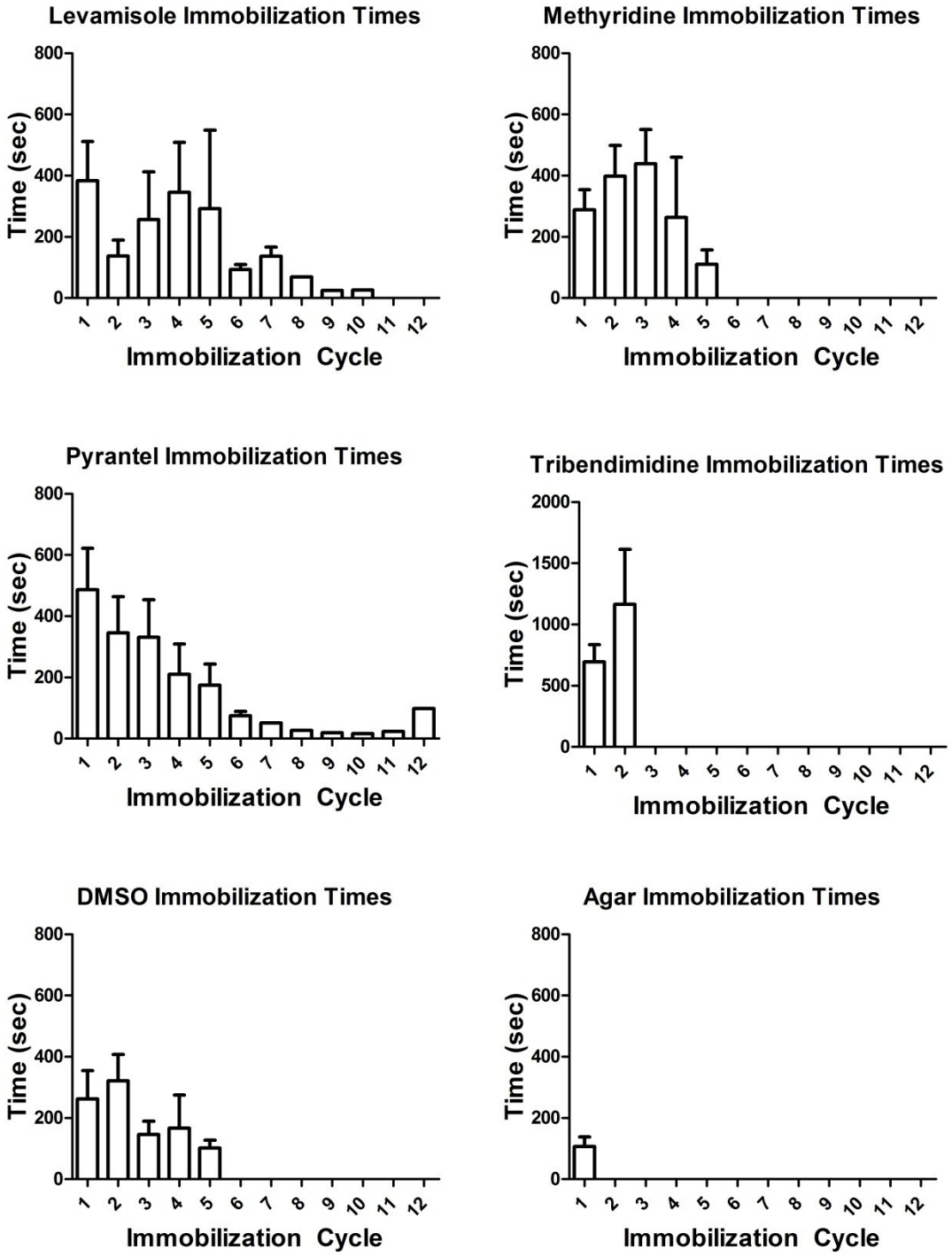

Figure 1.9: The observed median immobilization times for each immobilization period when *C.elegans* were exposed to a variety of drug conditions (levamisole, methyridine, pyrantel, tribendimidine, DMSO, and agar). All graphs except the tribendimidine immobilization times graph have the same axis units.

Based on the parameters we presented to quantify the effects of drug exposure on *C.elegans*, it would be useful to generate a performance measure summarizing all the results. Figure 9 categorizes the results of drug exposure in the microfluidic experiment. We decided to use five key parameters: curls per second, types of immobilization, mode frequency, number of active cycles, and duration of active cycles. With respect to the curls per second, three drugs that show similar effects are grouped as Group A (levamisole, pyrantel, tribendimidine), while the remaining three chemicals (methyridine, agarose, DMSO) are grouped as Group B. Regarding types of immobilization, methyridine and agarose are grouped as Group A , while tribendimidine and pyrantel are grouped as Group B. The number of active cycles are similar for levamisole and pyrantel (Group A), that for methyridine and DMSO (Group B), and that for tribendimidine and agarose (Group C). Active times are similar for levamisole and pyrantel (grouped as Group A), while methyridine and DMSO are grouped as Group B.

	Levamisole	Methyridine	Tribendimidine	Pyrantel	DMSO	Agar
Curls Per Second	Group A	Group B	Group A	Group A	Group B	Group B
Number of Active Cycles	Group A	Group B	Group C	Group A	Group B	Group C
Duration of Active Cycles	Group A	Group B	Individual	Group A	Group B	Individual
Types of Immobilizations	Individual	Group A	Group B	Group B	Group A	Group A
Mode Frequency	Group L	Group M	Group L	Group M	Not Analyzed	Not Analyzed

Table 1.1: Table of drug groupings based on observations from measured parameters in *C.elegans* behavioral analysis. Groupings of drugs that share traits across multiple parameters have been highlighted in red and blue.

Based on these drug groupings of shared parameters we can hypothesize that drugs what affect the *C.elegans* in similar manner do so using similar mechanisms such as chemical receptors or molecular modes of activity. This could allow us to identify an unknown drug based on its effect on *C.elegans* and without having to perform an expensive drug analysis to discover its composition. We can also use this information to detect which drugs act upon the same receptors or chemical pathways by observing which drugs cause worms to behave in similar manners across multiple observed parameters.

1.4 Discussion

In this chapter, we presented a microfluidic device for quantifying the effects of drug exposure on *C.elegans*. Four drugs were used for the experiments and key motility parameters were identified that delineate the differences in drug effects. Experimental videos were primarily analyzed manually and statistical differences were observed in the different motility parameters. To the best of our knowledge, such a detailed characterization of worm paralysis upon exposure to anthelmintics has not been studied in the scientific community. We feel that the microfluidic technology presented here will enlighten our understanding of worm behavior in the presence of drugs and unravel new biological phenomena that were not possible with traditional inhibition assays. Even though we investigated the behavioral changes in worm motility, additional biophysical studies could be performed to establish the link between individual drug mechanisms and the observed phenotype.

1.5 Reference

[1] Rankin, C.H., Beck, C.D.O. and Chiba, C.M., "Caenorhabditis elegans: A new model system for the study of learning and memory," *Behavioural Brain Research*, 37, pp. 89-92.

[2] Wicks, S.R. and Rankin, C.H. "The effects of tap withdrawal response habituation on other withdrawal behaviors: The localization of habituation in *C.elegans," Behavioral Neuroscience*, 111, pp.1-12. (1997).

[3] Kaletta, T., & Hengartner, M. O., "Finding function in novel targets: *C.elegans* as a model organism," Nature Reviews Drug Discovery, 5(5), pp. 387-399.

[4] O'Connell, D., "Worming a way to better drugs." *Nature Reviews Microbiology*, 4(8), pp. 568-569. (2006).

[5] Prichard, R. K., & Geary, T. G. "Drug discovery: Fresh hope to can the worms," *Nature*, 452(7184), pp.157-158. (2008).

[6] Gaba, S., Cabaret, J., Sauvé, C., Cortet, J., & Silvestre, A., "Experimental and modeling approaches to evaluate different aspects of the efficacy of Targeted Selective Treatment of anthelmintics against sheep parasite nematodes," *Veterinary Parasitology*, 171(3-4), pp. 254-262. (2010).

[7] Martin, R. J., Bai, G., Clark, C. L., & Robertson, A. P., "Methyridine (2-[2-methoxyethyl]-pyridine]) and levamisole activate different ACh receptor subtypes in nematode parasites: a new lead for levamisole-resistance," *British Journal of Pharmacology*, 140(6), pp. 1068-1076. (2003).

Chapter 2

Electro-Mechanical Screening of Nematodes

2.1 Introduction

2.1.1 Background

The field of microfluidics has significantly advanced in recent years, providing new insights and novel analysis methods in the fields of biology and medicine [1]. Of particular interest to our research, microfluidic systems are being sought for the rapid screening and manipulation of small microorganisms such as Escherichia coli, drosophila, and *C.elegans* [2-6]. This has further fueled research efforts in gene analysis, pest management, and combinatorial drug discovery.

Our research here is primarily geared towards discovering new microscale methods of sensing and manipulating two categories of nematodes (or worms): the non-parasitic *C.elegans* (Caenorhabditis *elegans*) and pig parasitic O. *dendatum* (Oesophagostomum *dendatum*). Continuing our discussion from the previous chapter where we demonstrated a microfluidic platform for screening chemical compounds on *C.elegans*, we now propose microfluidic schemes employing electrical and mechanical forces to manipulate these nematodes.

Development of such small-scale devices that use electro-mechanical forces will enable researchers to build high-throughput animal sorting systems that can be easily integrated and with minimal overhead cost.

2.1.1 Objectives

In this Chapter, we present three distinct microfluidic devices: (i) electrical valve to block or allow worm movement, (ii) maze structures to study worm interactions with angled, hard surfaces, and (iii) sinusoidal channels to sort worms based on their body vigor.

2.2 Methods and Procedures

2.2.1 Device fabrication

The abovementioned three microfluidic devices are fabricated using standard soft lithography. Even though their individual topologies are different, the three devices are all fabricated in a similar manner. Firstly, the device design is drawn in AutoCAD and sent to a vendor (Fineline Imaging, Colorado Springs, CO) for mask fabrication. The black-and-white masks are then used in soft lithography to produce a SU-8 photoresist (Microchem Corpation, Newton, MA) negative mold of the microfluidic device. The SU-8 is poured on a bare silicon wafer and spin-coated (spin at 2800 rpm; soft bake at 65 C for 5 minutes; repeat once) to create an 80 μm thick layer of photoresist. This photoresist is then exposed to near UV (375 nm) light (10 milliJoules per square centimeter for 50 seconds.) followed by a post exposure bake. The unexposed SU-8 is dissolved in a developing solution (Microchem Corpation, Newton, MA) and then hard baked (150 C for 15 minutes). PDMS prepolymer (Sylgar 184 Silicone Elastomer Kit, Dow Corning Corporation, Midland, MI) is then poured over the SU-8 mold and cured for 4 hours at 55 C. After curing, the hardened PDMS layer is peeled off the mold, cut to size, punched to create ports, and finally bonded to glass slides by exposing the PDMS device and glass slide to air plasma (Plasma Cleaner PDC-32G, Harrick Plasma).

2.2.2 Maintenance of the Nematodes

For this study, three strains of *C.elegans* are used: wildtype, acr-16, and lev-8 (Caenorhabditis Genetics Center (CGC) at University of Minnesota, St. Paul, USA). The *C.elegans* used in this experiment are cultured at room temperature on Nematode Growth Media (NGM) plates seeded with Escerichia coli OP50. During experiments, *C.elegans* are handpicked from the NGM culture plate using a platinum wire scoop and dropped in the entry port of a microfluidic device.

The *O. dentatum* worms used in these studies are of two different strains, Levamisole-sensitive (SENS) and resistant (LEVR) *O. dentatum*, and originally supplied by the Royal Veterinary and Agricultural School, Frederiksberg, Copenhagen. The worms are reproduced at six to nine months interval by passage in pigs at Iowa State University. The L2 larvae isolates are maintained between passages in tap water refrigerated at 11°C (changed every 2 - 4 months). To load the *O. dentatum* during experiments, a 1 mL syringe is filled with a suspension of *O. dentatum* in water and injected into the entry port of a microfluidic device.

2.2.3 Image Acquisition and Statistical Data Analysis

Images are recorded at a rate of 1 image per second using a Leica M205C and QImaging camera software. The microscope and imaging system were purchased from North Central Instruments, MN. Experimental recordings are performed for a finite time period, depending on the specific nature of the tests. The videos are saved in 1 terabyte external hard drive, and later analyzed either manually or by a custom image-tracking program. The extracted data is then processed by a statistical data analysis program, GraphPad Prism.

2.3 Results

2.3.1 Device 1: Electrical valve to block or allow worm movement

The microfluidic valve device is fabricated using the standard procedure mentioned previously (Section 2.2.1). The device comprises a central channel (length = 1 cm, width = 350 μm, height = 80 μm) with worm entry and exit ports at either end. The central channel is intersected by

thinner side channels (length = 500 μm, width = 25 μm, height = 80 μm) ending with smaller side ports for the placement of electrodes. Because of the device dimensions, any *C.elegans* that enters the central channel is restricted from entering into the thinner side channels. The Figure 2.1 shows the microfluidic device and a three-dimensional view of the testing system.

After the microfluidic device fabrication, liquid agar is injected into the central channel. Platinum electrodes (length = 2 cm) are inserted into two selected side ports and connected to an Agilent E3630A power supply to generate the electric field. The distance between two side channels was 2 mm. The electrical conductivity and the current between the electrodes are checked by an Agilent 34401A digital multimeter. Our initial experiments gave us a good understanding of the voltage and current levels that could be used in the setup. The voltage level was kept at 10 volts DC across the electrodes (0 V at the anode and -10 at the cathode) and an electric field of 33.33 V/cm. With the agarose gel having an approximate resistance of 0.98 MOhm between the electrodes, the total current in this case is around 10 μA, which is lower than the minimum current that is known to damage the *C.elegans*. Thereafter, L4 stage *C.elegans* are dropped into the entry port and allowed to migrate into the central channel. We observed that worms do not prefer to enter channel regions where the electric field is incident to its direction of movement. On the other hand, worms move freely in channel regions with no electric field or in channel regions where the electric field is in the same direction as its movement. Thus a virtual electrical valve is created on-chip for *C.elegans* by changing the direction of the electric field in the central channel.

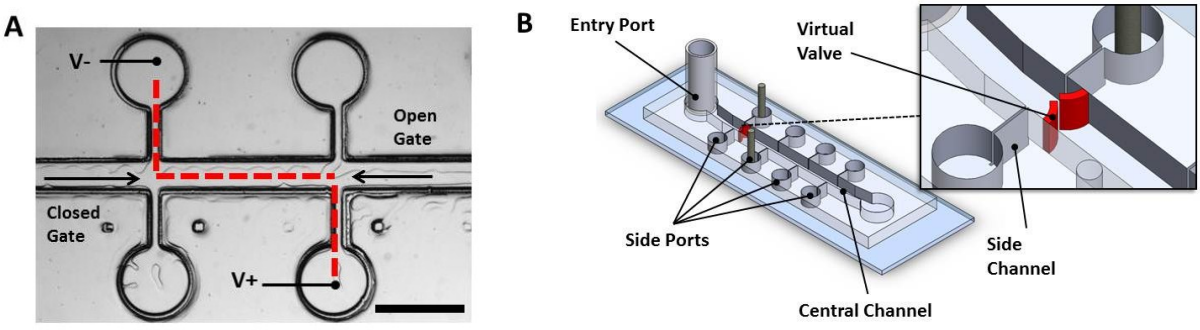

Figure 2.1: A) Close up of virtual valve and arrangement of electrodes (V- & V+) in reference to gate (electric field shown in red). B) 3D design of the electric valve system.

Our results are based on showing the effectiveness of the electrical valve in allowing or blocking *C.elegans* movement within a particular section of the central channel. The first attribute of the system observed in this study is the ability to 'hold' (i.e. to block) worms from passing through the virtual valve. The worm percentage held for each strain of *C.elegans* in this study is plotted in Figure 2.3 A. We notice that the virtual valve held almost all *C.elegans* with minor variations between strains; 100% of the wildtype, 95+-5% of the acr-16 mutant, and 100% of the lev-8 mutants were held (n=21 for each strain and each worm was examined for 3 experimental trials). In addition to examining the ability of the virtual valve to hold *C.elegans*, the penetration depth of each *C.elegans* into the region of the virtual valve is analyzed. This penetration depth is the longitudinal distance from the cathode electrode port to the farthest point that the *C.elegans* moved into the virtual valve region (as shown in Figure 2.2). Based on the average stopping distances for all tested strains of worms, the stopping distance for most worms is approximately 175 μm, with only a few nematodes penetrating much further (400 μm) as detailed in Figure 2.3 B.

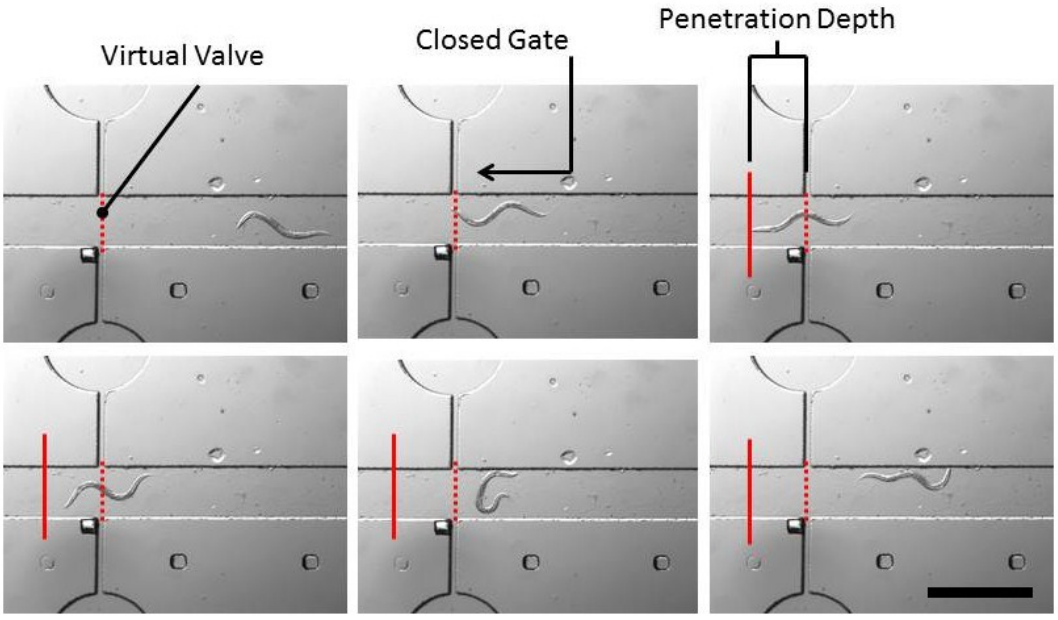

Figure 2.2: Diagram showing a usual *C.elegans* interaction with the virtual valve and how penetration depth is measured. Dotted Red line is the virtual value and the solid red line is the furthest point of penetration the worm achieved. The penetration depth is the distance between the virtual gate and the furthest penetration point. Scale bar is 1 mm.

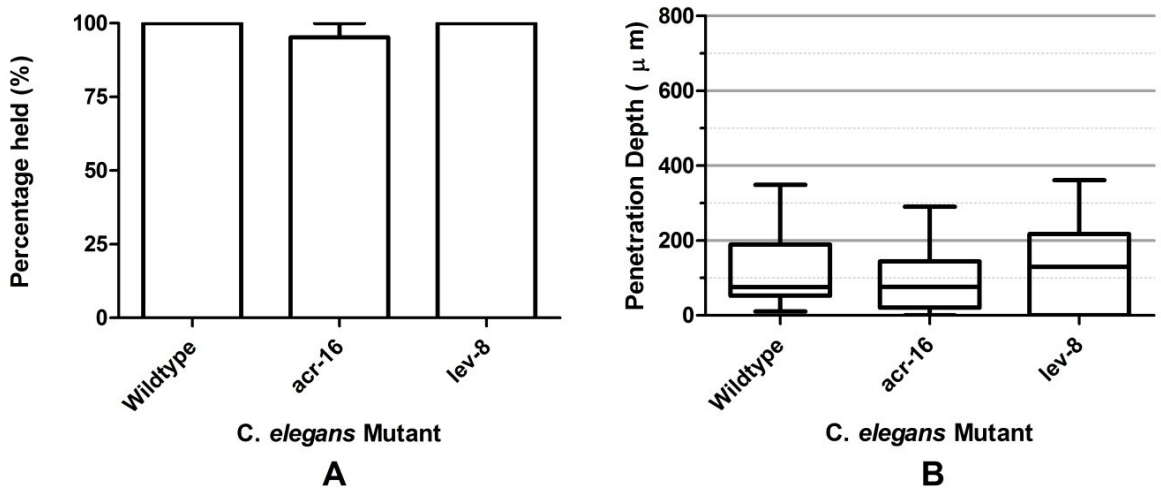

Figure 2.3: A) Chart displaying the percentage of worms held by the electric field for the different *C.elegans* mutants. B) Graph describing the penetration depth into the electric field achieved by different *C.elegans* mutants.

To ensure that the observed health of the worm is not affected by exposure of electric fields, we measured the worm centroid velocity before and after coming in contact with the virtual valve. Before coming into contact with the virtual value the different strains had the following average forward velocities: wildtype = 238.8 ± 17.2 μm/s, lev-8 = 227.6 ± 15.4 μm/s, and acr-16 = 242.3 ± 28.9 μm/s; n=10 for each strain. After contact with the virtual value the strains had the following velocities wildtype = 245.9 ± 29.9 μm/s, lev-8 = 235.8 ± 27.7 μm/s, and acr-16 = 222.5 ± 19.3 μm/s; n=10 for each strain. The differences between the before and after contact forward velocities were shown to not be a significant change ($p<0.05$; ANOVA test).

In conclusion, we developed a virtual valve system that is purely electrical in nature and has no mechanical or moving parts. The operating principle of our electrical valve is based on a simple fact that, in an electric field region, *C.elegans* are attracted towards the cathode (or negative polarity) terminal but do not prefer to enter channel regions where the field lines are incident to its head [7-10]. Our electrical valve has a nearly 100% blocking rate and does not produce any harmful effects on the animals. Such an all-electrical valve could be combined in multiple configurations to produce an all-electrical method of controlling the locomotion of multiple worms in an integrated system. Unlike pneumatic valves, our device requires a single mask fabrication step and no extra mechanical parts (such as syringe pumps and fluid tubings).

2.3.2 Device 2: T-Maze structures to study worm interactions with angled, hard surfaces

The second microfluidic device is fabricated using the standard procedure mentioned previously (Section 2.2.1). Here our goal is to characterize worm behavior when it is challenged through angled surfaces, such as those encountered in their natural soil environment. Because *C.elegans* are deprived any limbs or eyes, they primarily rely on sensory neurons in their mouth region to maneuver through hard or soft surfaces [10-14]. Numerous studies have delved into the role of chemotaxis (i.e. taxis by smelling chemical) in guiding the direction of worm movement and have modeled their chemosensory pathways [15-20]. But the role of mechanical cues in guiding the direction of worm movement is largely unknown, and we aim here to characterize this interesting behavior using microfluidics and real-time imaging.

Two types of angled interfaces are designed: single T-maze structures with varying angles of intersection and a sequence of multiple T-maze structures of pre-defined angles of intersections. The first structure, single T-maze, comprises a central channel (Length = 10 mm, Width = 300 µm, Height = 80 µm) with an entry port at one end and bifurcating into two shorter side channels (Length = 2 mm, Width = 300 µm, Height = 80 µm) with their individual exit ports. In the different designs, the side channel intersects the central channel at angles of 15, 30, 45, 60, 75 or 90 degrees. The second structure, sequenced T-maze, is a series of five T-maze (Width = 300 µm, Height = 80 µm), each having an exit port on the left side and leading into the next T-maze on the right side. Each T-maze in the series either has the same intersection angle or decreasing intersection angles following the first 90 degree intersection. Figure 2.4 shows a diagram of both T-maze devices used in this study.

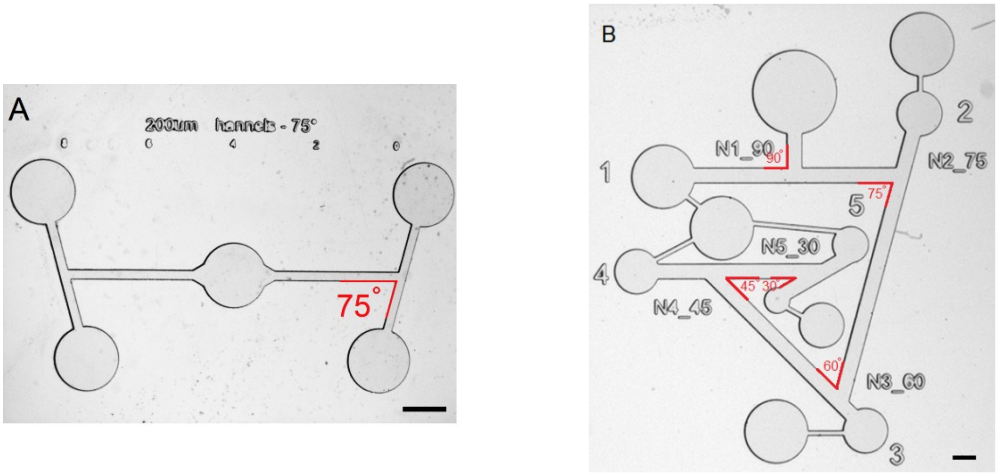

Figure 2.4: A) Photograph of single 75 degree T-maze device and B) Photograph of Sequential decreasing angle T-maze device with angles of intersections in red. Scale bar for both A and B is 100 µm

After the microfluidic devices are fabricated, 0.8% agar is injected into the microchannels. Because of the diverging channel geometries, it is easy to trap air bubbles at random locations in the device that may impede or obstruct the worm movement. To avoid any air bubbles, the filling is continued several times till no air bubbles are observed. Next, either L4-stage *C.elegans* are hand-picked and dropped into the entry port or *O. dentatum* are loaded into a syringe and injected into the entry port of the device. The worms are allowed to migrate freely without any chemical or electrical stimulation and their movement is recorded with a Leica microscope as described before (Section 2.2.2).

We manually analyzed the recorded videos and calculated the percentage of worms that would turn right or left upon impacting the intersection wall of a single T-maze. Figure 2.5 shows the percentage of worms that made a left or right turn in the different T-maze structures. When the intersection angle of the T-maze is 90 degrees, the both *C.elegans* and *O. dentatum* showed roughly 50% preference for a right or left turn. As the intersection angle is increased from 15 to 90 degrees (by using different T-maze devices), the percentage of worms making a left turn decreases almost linearly (and inverse for turning right). These results allow us to build a probabilistic model for the turning behaviors of *C.elegans* and *O. dentatum* simply based on the intersection angle of a T-maze.

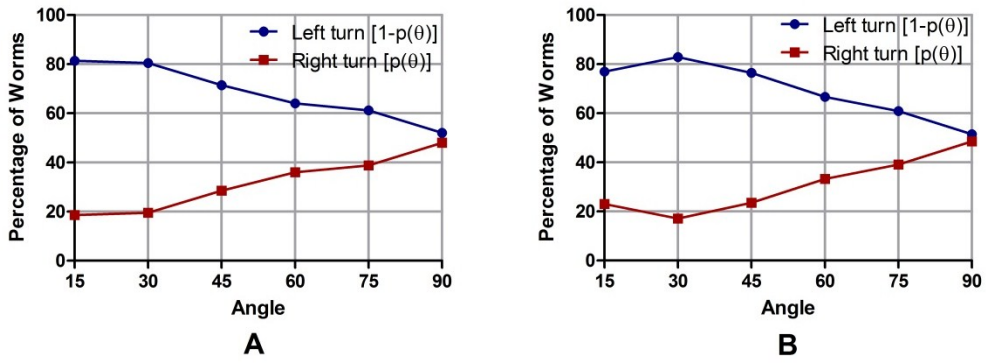

Figure 2.5: Observed percentages of worms turning either left of right the angle of the intersection, Θ, is increased from 15 degrees to 90 degrees.

After characterizing the turning behavior of worms using single T-maze structures, we realized that the most important factor guiding the direction of worm movement is the intersection angle of a T-maze. To further verify that the intersection angle still plays a major role in guiding worm

directionality, we designed a sequenced T-maze structure. Here a series of five T-maze structures are connected serially and, at each intersection angle, the worm is provided an option to exit the maze. We tested worm locomotion in three types of sequenced T-maze structures: one where all intersection angles are 60 degrees, one where all intersection angles are 90 degrees, and one where the intersection angle keeps decreasing from 90 degrees.

During experimentation, worms are dropped into the entry port and allowed to navigate through the T-maze structures. After 30 minutes of recording, the number of worms that collect at the different exit ports are counted. Using the simple probabilistic model built earlier using single T-mazes, we are also able to calculate the probability of finding a worm in a given exit port. Both the theoretical and experimental values are plotted in Figure 2.6. To determine the percentages of worms that turned left or right at each intersection we monitored the exit ports on the device and counted the number of worms that arrived at each port; once a worm arrived in a port it was no longer tracked. Using this technique to count the number of worms turning at each intersection we observed worms behavior in microfluidic devices with angles of 60 degrees, with 90 degrees, and 90, 75, 60, 45, 30, and 15 degrees in series. The percentage of *C.elegans* and *O. dentatum* turning in each of these cases is shown in Figure 2.6. There was no significant difference in the theoretical and experimental results. This further reaffirms our previous hypothesis that the intersection angle plays an important role in guiding worms through angle maze structures.

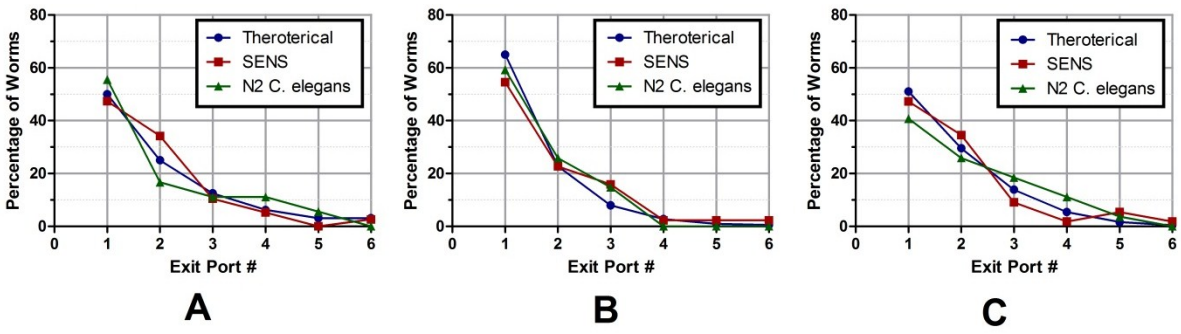

Figure 2.6: Percentages of worms collected at each exit for each sequenced T-maze: (A) sequence 90 degrees T-maze, (B) sequence 60 degrees T-maze, and (C) sequence decreasing T-maze.

Besides characterizing the turning behavior of worms, we investigated their body behavior at the intersection of each T-maze. The recorded videos were reexamined to understand how the worms made impact with the PDMS wall at the intersection regions. Then we tried to classify the

observed body behavior into discrete categories for the ease of understanding. In the case of *C.elegans*, the possible discrete states of body impact follow the pattern: physical impact, slide on impact, slide off surface, back off body, back off head, turn head around, and leave intersection. In the case of *O. dentatum*, the possible discrete states of body impact are: physical impact, slide on impact, slide off surface, dig head in, back off head, back off body, and leave intersection. Analyzing the impacts from all videos, we generated the following Figure 2.7 to describe their behavior.

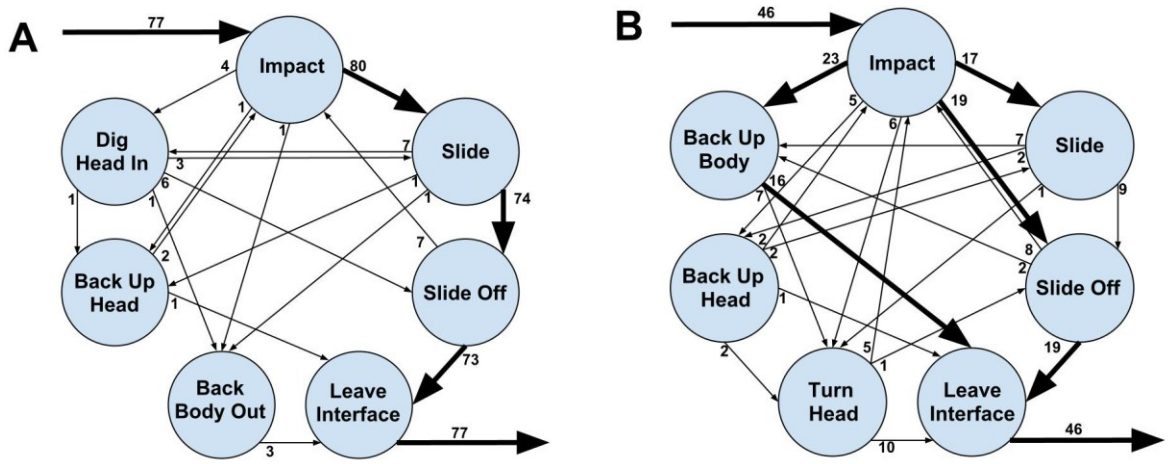

Figure 2.7: Flow diagrams for the interactions for A) *O. dentatum* and B) *C.elegans* when impacting and navigating a T-maze intersection. The number of worms transitioning from one state to the next is labeled at the start of each arrow. Bold arrows denote primary paths through the flow diagrams.

Based on this impact analysis, we observe that *C.elegans* and *O. dentatum* do not have similar body behavior upon reaching the intersection region. *O. dentatum* perform a simple impact, slide, and slide off behavior at intersection regions. In contrast, *C.elegans* exhibit a wide range of actions upon reaching the intersection region, with no single path describing a majority of worm turn actions. In addition, *C.elegans* also demonstrated a “probing” behavior where they probe the surface multiple times with their head. This probing behavior is distinctly absent in *O. dentatum*. These observed differences may, in turn, be related to the larger body size and more developed neurosensory of *C.elegans* compared to those of *O. dentatum*.

2.3.3 Device 3: Sinusoidal channels to sort worms based on their body vigor

The third device used to study the mechanistic behavior of *C.elegans* consists of a series of sinusoidal channels. We have earlier seen that worms move in a sine-wave fashion, and the amplitude or wavelength of their inherent locomotion cannot be changed externally [21-27]. We hypothesized that, if worms are restricted in tight sinusoidal channels, they would have to conform their body shape according to the channel geometry. Thus we would be able to test the adaptability of different worm mutants, each having different amplitude and wavelength of inherent locomotion.

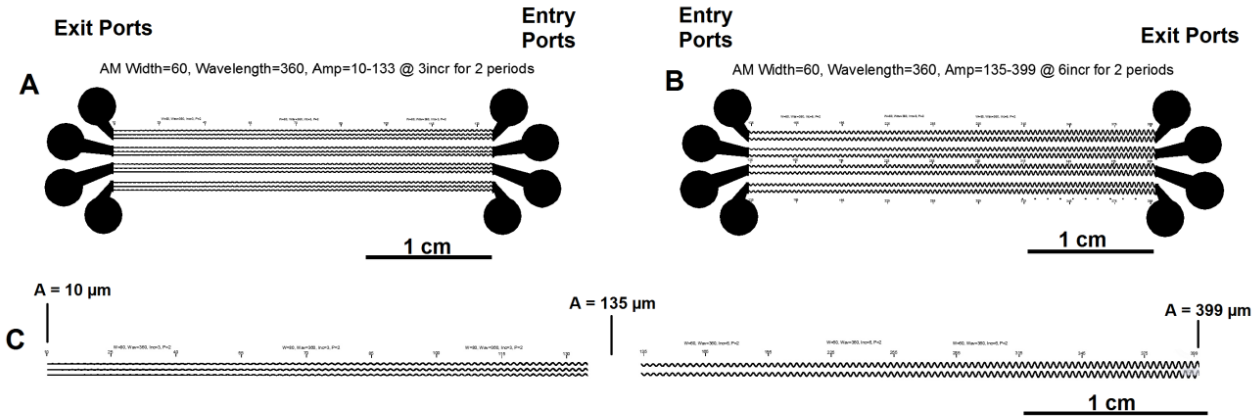

Figure 2.8: Design of sinusoidal channels microfluidic devices for amplitudes of A) 10 – 135 µm and B) 135 – 399 µm. C) Zoomed view of channels for both A and B.

The device is fabricated in the same method as previously described in Section 2.2.1. Each device consists of multiple sinusoidal channels of fixed wavelength but varying amplitude. Each sinusoidal channel has a wavelength of 360 µm and amplitude varying from 135 µm to 10 µm or from 135 µm to 399 µm. The design of the microfluidic device is shown in Figure 2.8. During the experiment, the sinusoidal channels are filled with standard M9 buffer and L4 stage wildtype, lev-8, or unc-38 *C.elegans* are dropped into the entry port. Once into the sinusoidal channel, the worms are allowed to migrate through the channel without any external electrical, chemical, or mechanical manipulation. As the worms traverse the sinusoidal channels, their movement is recorded using the method described in Section 2.2.2. Analyzing the videos of the *C.elegans* as they traverse the sine channel microfluidic devices, we were able to quantify a wide range of behavioral characteristics of the different worm strains. In particular, the average forward velocity, range of contact angle, and cut-off region were examined for the three different strains in this study.

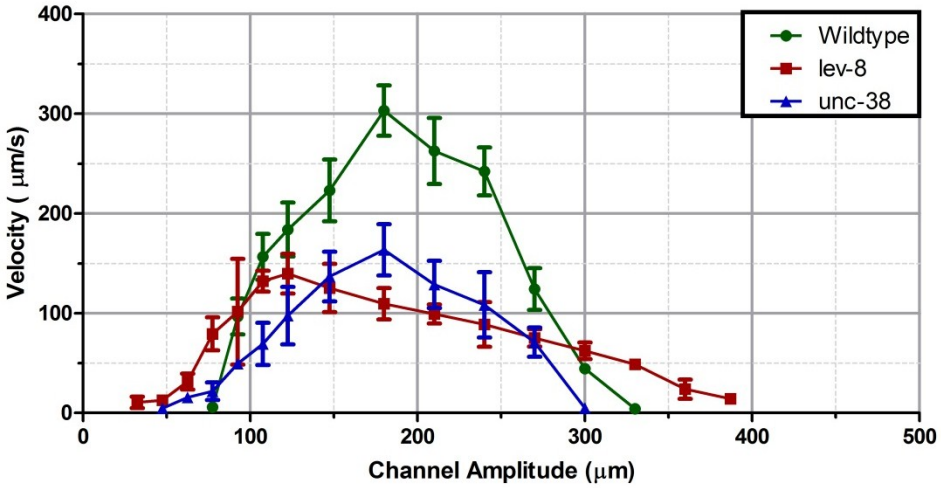

Figure 2.9: This graph displays the *C.elegans* forward velocities within sinusoidal channels with changing amplitude from 10 to 399 μm.

We noticed that the forward velocity can be used to describe the ease at which the worms are able to navigate the sine channels; the higher the speed, the better suited the worm is to the channel. For the regions of the channel where the worms move slower the worms must contort their body in the channel to move forward in the channel for low amplitudes or simply to squeeze through the high amplitude sections of the channel that do not match the worm's natural sinusoidal motion. Figure 2.9 shows the average forward velocity of *C.elegans* (wildtype, *lev-8* and *unc-38*) as a function of the channel's amplitude. For each strain, the velocity curve has a peak (303+-25.3 μm/s for wildtype, 139.60+-19.8 μm/s for *lev-8*, and 163.42+-25.7 μm/s for *unc-38*, mean+-S.E.) at a certain amplitude (180 μm for wildtype, 122.5 μm for *lev-8*, and 180 μm for *unc-38*, n=15–20, N=3) and decays on either side of this amplitude. From this data we can see the average forward velocity for wildtype is the highest out of all mutants, with a peak at the amplitude 180 μm, and exhibits a standard Gaussian distribution. The unc-38 mutant has a similar Gaussian distribution and peak at 180 μm, but only at 53% of the speed of the wildtype. Lev-8 mutants exhibited a skewed distribution in contrast to the other mutants and a velocity similar to that of unc-38.

In an attempt to relate the forward velocity measured in channels with those on planar, open space, we quantified the amplitude and wavelength of inherent locomotion on agarose plates [22]. The three strains of *C.elegans* mutants are examined on agarose plates to determine their natural amplitude (A) and wavelength (λ) ratio. The A/λ ratio for the three strains (n=12–15) on agarose plates are: A/λ =0.46 for wildtype, A/λ =0.33 for *lev-8*, and A/λ =0.54 for *unc-38*. From

Figure 2.9, the peak velocities occur at channel regions where A/ λ =0.5 for wildtype, A/ Lambda =0.34 for *lev-8*, and A/λ =0.5 for *unc-38*. Where the natural A/λ ratios of the worms match closely with that of the channel, the worm velocity is the greatest. This agrees with our earlier expectation that the *C.elegans* move fastest in channel regions whose dimensions match their natural sinusoidal wave.

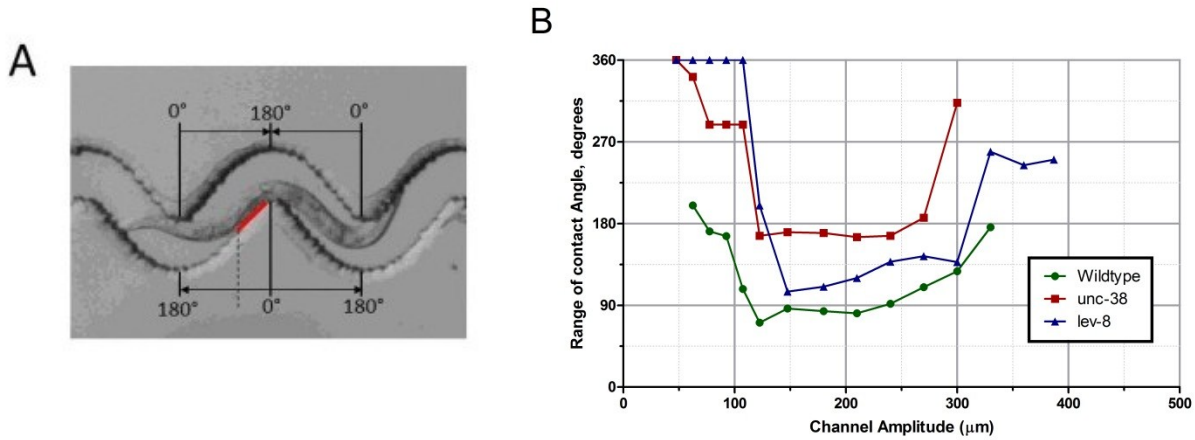

Figure 2.10: A) Image showing a *C.elegans* in the sinusoidal channel and the criteria used to measure range of contact angle. The contact point of the worm with the side wall (shown in red) furthest from the central peak is taken as the greatest point in the range of contact angles. B) The range of contact angle *C.elegans* make while maneuvering through sinusoidal channels.

As worms navigate through the sinusoidal channels, they push different regions of their body against the PDMS sidewalls to generate the forward thrust. In the extreme cases when the channel amplitude is very small or very large, one would expect the worm to struggle a lot harder [27]. In these cases, most of its body would be touching the sidewalls. Reexamining the videos, we marked regions of the worm body that made contact with the channel sidewalls. We used these points of contact to define the range of contact angle where the worm's body had a specific posture (i.e., where body's middle section is centered at the channel's crest and the head and tail regions are outside the two troughs on either side of the crest) as shown in Figure 2.10 A. Then we identified the two extreme contact points of the body's middle section and extrapolated them individually to a vertical line corresponding to the channel's crest. The angle between these two lines is denoted as the range of contact angle and is measured for individual worms at different sections of the sinusoidal channel.

In Figure 2.10 B we observed that when most worms strains were within the optimal amplitude range for motion (region of the sine channel where the worm have the greatest forward

velocity), they make less contact with the sidewall of the microfluidic device and have a smaller range of contact angle. All wildtype and unc-38 are within their optimal ranges when the range of contact was less than 180 degrees, but lev-8 showed optimal motion when have its highest range of contact angles. Wildtype worms exhibited the lowest range of contact angles for the entire range of channel amplitudes. This finding agrees with the earlier observation that wildtype worms had a greater forward velocity than all other strains. Unc-38 performed similar to wildtype, but at higher range of contact angles overall. Of interest are the contact angles of the lev-8 mutant, which has its highest forward velocity in the range of channel where it has the greatest range of contact angle immediately before where it has its lowest range of contact angles, approximately 100-150 µm.

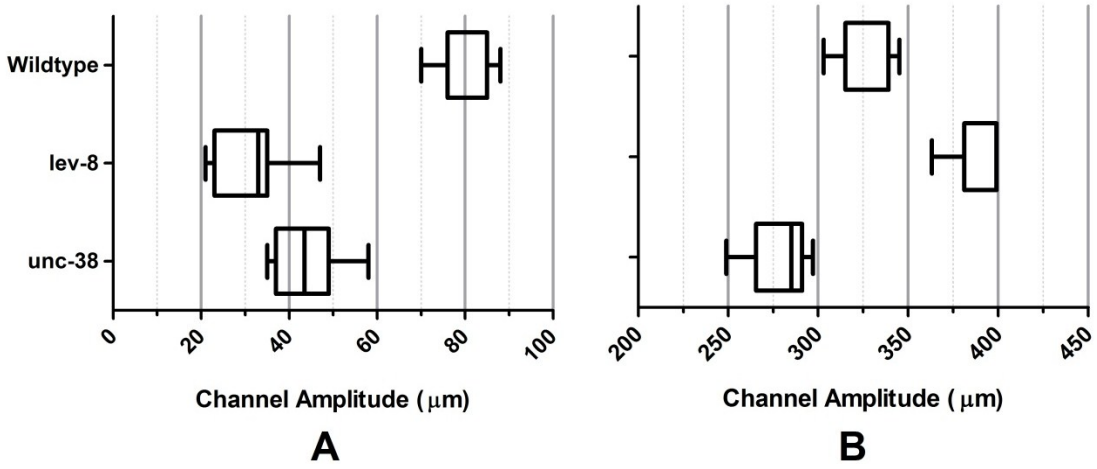

Figure 2.11: This Figure shows the A) low cut-off range and B) high cut-off range of amplitudes which *C.elegans* can traverse within the sinusoidal microfluidic device. Amplitudes above the low cut-off region and below the high cut-off region can be navigated by the worms; beyond these amplitudes, the worms are unable to pass through the channel.

Figure 2.11 shows the cut off regions for the different *C.elegans* mutants. The cut-off region is defined as the channel region beyond which a worm is unable to pass through. The first half of the graph represents the cut-off region for sinusoidal channels having the lower amplitude range, while the second half of the graph corresponds to the cut-off region for sinusoidal channels having the higher amplitude range. Lev-8 mutants display the widest range of amplitudes of the three mutants. In other words, they could traverse a wider range of channel amplitudes. The lower cut-off for the individual strains are 78.73+-6.6 µm for wildtype, 31.41+-8.0 µm for *lev-8*, and 44.43+-8.1 µm for *unc-38* (mean+-S.E., n=15–20, N>3). The upper cut-off

for the individual strains are 322.7+-14.1 μm for wildtype, 390.7+-14.3 μm for *lev-8*, and 278.9+-15.6 μm for *unc-38* (mean+-S.E., *n*=15–20, *N*>3).

The modulated amplitude sine channel provides us with an accurate means to analyze the vigor of different *C.elegans* mutants, in this study wildtype, lev-8, and unc-38. By using sinusoidal channels, we were able to restrict the motion of *C.elegans* and force them to navigate within the channel. By decreasing or increasing the channel amplitude, we were passively able to differentiate mutants that can exert less or more force without any sophisticated system.

2.4 Discussion

In this chapter, we presented three devices for isolating and highlighting a certain electrical or mechanical behavioral aspect of nematodes. The use of microfluidics with real-time imaging provided us a unique advantage of probing worm behavior with high spatial and temporal resolution. Even though some of our results were extracted manually, we envision the development of automated image-tracking programs that could eliminate human intervention. Overall we were able to show that nematodes, which are traditionally classified into genetically distinct groups, may show differences in behavioral patterns. This link between the genetic makeup of an organism and its associated behavioral patterns is imperative in today's next-gen sequencing era.

2.4 Reference

[1] Whitesides, G. M., "The Origins and the Future of Microfluidics," *Nature*, *442*, 368-373. (2006).

[2] Melin J, Quake SR. "Microfluidic Large-Scale Integration: The Evolution of Design Rules for Biological Automation" *Annu. Rev. Biophys. Biomol. Struct.* 36:213-31

[3] Weibel, D.B., DiLuzio, W.R., and Whitesides, G.M., "Microfabrication Meets Microbiology," *Nature Reviews Microbiology*, *5*, 209-218 (2007).

[4] Weibel, D.B., DiLuzio, W.R., and Whitesides, G.M., "Combining Microscience and Neurobiology", *Current Opinion in Neurobiology*, *15*, 8-Jan. (2005).

[6] Kim, N, Dempsey, C, Zoval, J, Sze, J, Madou, M, "Automated microfluidic compact disc (CD) cultivation system of Caenorhabditis elegans," *Sensors and Actuators B: Chemical*, 122(2), 511-518. (2007).

[7] Gabel, C.V., Gabel, H., Pavlichin, D., Kao, A., Clark, D., and Samuel, A., "Neural Circuits Mediate Electrosensory Behavior in *Caenorhabditis elegans*," *The Journal of Neuroscience*, 27(28):7586 –7596. (2007).

[8] Rezai, P., Siddiqui, A., Selvaganapathy, P., Gupta, B., "Electrotaxis of C.elegans in a microfluidic environment," *Lab on a Chip*, 10, 220–226. (2010).

[9] Rezai, P., Siddiqui, A., Selvaganapathy, P., Gupta, B., Behavior of Caenorhabditis elegans in Alternating Electric Field and its Application to their Localization and Control, *Applied Physics Letters*, 96, 153702. (2010).

[10] Petersen, M.B., Craven, J., Bjørn, H., and Nansen, P., "Use of a migration assay for the separation of adult pyrantel-susceptible and -resistant Oesophagostomum dentatum," *Veterinary Parasitology*, 91, 141-145. (2000).

[11] Kotze, A.C., Le Jambre, L.F., and O'Grady, J., "A modified larval migration assay for detection of re- sistance to macrocyclic lactones in Haemonchus contortus, and drug screening with Trichostrongylidae parasites," *Veterinary Parasitology*, 137, 294-305. (2006).

[12] Daugschies, A. and Ruttkowski, B., "Modulation of migration of Oesophagostomum dentatum larvae by inhibitors and products of eicosanoid metabolism," *International Journal for Parasitology*, 28, 355-362. (1998).

[13] Lorimer, S.D., Perry, N.B., Foster, L.M., Burgess, E.J., Douch, P.G.C., Hamilton, M.C., Donaghy, M.J., and Mc- Gregor, R.A., "A Nematode Larval Motility Inhi- bition Assay for Screening Plant Extracts and Natural Products," *Journal of Agricultural and Food Chemistry*, 44, 2842-2845. (1996).

[14] Wang, W., Shor, L.M., LeBoeuf, E.J., Wikswo, J.P., Tag- hon, G.L., and Kosson, D.S., "Protozoan Migration in Bent Microfluidic Channels," *Applied and Environmental Microbiology*, 74, 1945-1949. (2008).

[15] Lockery, S.R., Lawton, K.J., Doll, J.C., Faumont S., and Coulthard, S.M., "Artificial dirt: Microfluidic substrates for nematode neurobiology and behavior," *Journal of Neurophysiology*, 99, 3136-3143. (2008),

[16] Park, S., Hwang, H., Nam, S.W., Martinez, F., Austin, R.H., and Ryu, W.S., "Enhanced *Caenorhabditis elegans* locomotion in a structured microfluidic environment," *PLoS One*, 3, e2550. (2008).

[17] Chronis, N., "Worm chips: Microtools for *C.elegans* biology," *Lab on a Chip*, 10, 432-437. (2010).

[18] Crane, M.M., Chung, K., Stirman, J., and Lu, H., "Microfluidics-enabled phenotyping, imaging, and screening of multicellular organisms," *Lab on a Chip*, 10, 1509-1517. (2010).

[19] Rohde, C.B., Zeng, F., Gonzalez-Rubio, R., Angel, M., and Yanik, M.F., "Microfluidic system for on-chip high-through-put whole-animal sorting and screening at subcellular resolution," *Proceeding of the National Academy of Sciences of the United States of America*, 104, 13891-13895. (2007).

[20] Qin, J. and Wheeler, A.R., "Maze exploration and learning in *C.elegans," Lab on a Chip*, 2007, 7, 186-192.

[21] Gray, J., and Lissmann, H. S., Journal of Exp. Biol. 41, 135 (1964).

[22] Karbowski, J., Cronin, C., Seah, C., Mendel, J., Cleary, D., and Sternberg, P., "Conservation rules, their breakdown, and optimality in *Caenorhabditis* sinusoidal locomotion," *Journal of Theoretical Biology*. 242, 652-669 (2006).

[23] Jung, S., "Atomization patterns produced by the oblique collision of two Newtonian liquid jets," *Physics of Fluids*. 22, 031903 (2010).

[24] Juarez, G., Lu, K., Sznitman, J., and Arratia, P.E., "Motility of small nematidesin wed granular media," *Europhys. Lett*. 92, 44002 (2010).

[25] Sznitman, J., Purohit, P., Krajacic, P., Lamitina, T., and Arratia, P.E., "Mterial Properties of Caenorhabditis elegans swimming at Low Reynolds Number," *Biophysical Journal*. 98, 617 (2010).

[26] Fang-Yen, C., Wyart, M., Xie, J., Kawai, R., Chen, S., Kodger, T., Wen, Q., and Samuel, A.D.T., "Biomechanical analysis of gait adaptation in the nematode *Caenorhabditis elegans*", *Proc. Natl. Acad. Sci. USA* **107**, 20323-20328 (2010).

[27] Lockery, S.R, Lawton, K.J., Doll, J.C., Faumont, S., and Coulthard, S.M., "Artificial Dirt: Microfluidic Substrates for Nematode Neurobiology and Behavior,"J. Neurophysio. 99, 3136 (2008).

Chapter 3

Electronic Platform for Culturing Neuronal Cells

3.1 Introduction

3.1.1 Background

Studies on the architecture and functioning of the human brain pose daunting challenges to scientists. As brain signals arise from numerous interconnected neurons, researchers have developed various schemes to cultivate and study neuronal cultures in vitro [1-10]. Cell migration is an important parameter of study in these in vitro neuronal cultures, which basically analyzes the ability and rate of live cells to migrate towards a known stimulus. While studying patterns of cell migration, we can envision how the brain responds to stimuli, injury, and changes in body fluid compositions. Furthermore, with a greater understanding of cell behavior, we can discover how neuro-pathological illnesses arise and how alternate treatments can be developed to combat these illnesses.

Classical methods of characterizing neuronal cell migration rely on cultivating cell populations in incubation chambers and taking images at fixed time intervals (usually every 12 or 24 hours).

After the end of the growth period, cells are fixed and stained for fluorescence studies. This method of cell analysis has been widely adopted by the scientific community because of its simplicity and reliability. Some limitations of this technique include low image-capture rate, risk of contamination associated with frequent removal of cell cultures from incubation chamber, and cost of human labor. Today a number of companies have emerged that sell cell culture/imaging systems. Such systems are usually expensive (> $100k) because of the level of automation and sophistication they incorporate.

As an alternative to the classical methods of characterizing cell migration, we propose an electronic biosensor to perform the same function. The proposed electronic system will be capable of detecting the position, size, and surface adherence of neuronal cells by electrically sensing the amount of surface charges from embedded field effect transistors (FET) (rather than by visual analysis). Our integrated chip contains arrays of CMOS floating-gate FETs, previously developed by our group at Iowa State University [1]. Our group had earlier shown that the floating-gate FET devices could measure and differentiate charged amino acids placed on its surface. The electronic readout of the FET devices was performed using a HP 4145 Semiconductor Parameter Analyzer, which is capable of simultaneously applying required voltages and measuring the current from individual devices. One attempt was also made to culture neuronal cells on the integrated chip and the cells appeared to have survived for around 48 hours. However, the health of the cell population was not clearly assessed.

Following the above-mentioned progress made by our group, we attempted to enhance the electronic readout capabilities of the integrated chip and grow sustainable, viable cell cultures on their surface. Currently, the HP 4145 is used to measure response of individual transistors but is incapable of reading the performance of an array of transistors. Furthermore the HP 4145 is bulky and a portable, stand-alone system is required to accompany the incubation chamber. Besides, we will focus on methods of improving chip surface modifications for better cell cultures on electronic chip surfaces with continuous recording.

3.1.2 Objectives

The objective of this project is to develop electronic readout system that will use the CMOS floating-gate biosensor previously developed by our lab to sense real-time neural cell migration. This requires the design of an electronic readout system to analyze the biosensor, incorporation of chip modification techniques to enhance cell growth conditions, and an analysis of surface treatments to support a viable culture of neuronal cells on the CMOS floating-gate biosensor.

3.2 Methods and Procedures

3.2.1 CMOS Floating-gate Biosensor

The CMOS floating-gate biosensor was developed at Iowa State University. This biosensor was fabricated through an outside vendor (MOSIS Integrated Circuit Fabrication Service, Marina del Rey, CA) and housed within a standard 40-pin case. Design of the CMOS biosensor's sensing surfaces are shown in Figure 3.1.

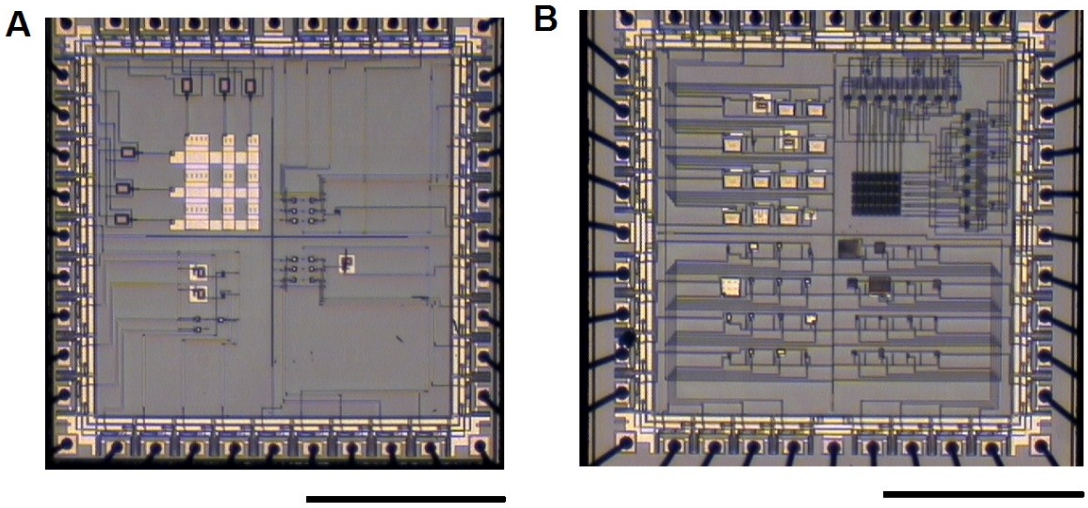

Figure 3.1: Overhead photographs of two of the CMOS biosensor designs: A) T7BL-AJ and B) T78J-AG. These images show the sensing surfaces of the individual FETs and FET arrays of the CMOS biosensor. Scale bar is 1 mm.

The CMOS floating-gate biosensor is essentially a very sensitive charge sensor. When charged molecules are placed on its surface, the threshold voltage of the biosensor device changes. This change is detected by measuring the output current of the device. The differential threshold voltage can be mathematically correlated to the amount of surface charges on the chip surface. This biosensor has been shown to accurately detect poly-L-lysine, poly-L-histidine, polyglutamic acid, poly aspartic acid, poly styrenesulfonic acid sodium salt, and poly diallyldimethyl ammonium chloride solutions on the biosensing surface [1]. As the surfaces of cells are negatively charged, this biosensor chip could be able to detect the presence of neuronal cells on its surface.

Prior testing of the biosensor has been performed using the HP4145 Semiconductor Parameter Analyzer. The HP4145 essentially has four outlets, each capable of applying a voltage (or current) and measure the output voltage (or current). This instrument has been widely used to characterize the performance of transistors. Even though this instrument is suited for single device testing, it is bulky and difficult to integrate with any cell incubation chambers. There are also the same limitations with cell migration studies as discussed before, such as manual intervention, lack of parallel readout of multiple devices, and risks of sample contamination.

3.2.2 Microfluidic Reservoirs for CMOS Floating-gate Biosensor

The first attempt of growing cells on the CMOS floating-gate biosensor was done in 100 mm petri plate that housed the entire chip. Within this petri plate, adult hippocampal progenitor cells (AHPCs) were suspended within culture media and manually plated onto the chip surface. Small amount of deionized (DI) water was added to the base of the container to reduce fluid evaporation. This setup functioned satisfactorily for cell growth but was difficult to connect to the electronic hardware and posed risks of exposing the cell culture to the outside environment.

To modify the existing fluidic system, a microfluidic reservoir comprising a 50 mm petri plate was chosen and attached to the top of the biosensor using superglue. A hole was drilled into the bottom of the chamber and the interface between the culture chamber and the biosensor was spanned by PDMS (Sylgard 184 Silicone Elastomer Kit, Dow Corning Corporation, Midland, MI) poured into the chamber. The PDMS directly above the biosensor is cut away to expose only the biosensing surface (2.2 mm x 2.2 mm). By adding a chamber to the top of the biosensor, a constant sterile environment for the cell culture is established rather than enclosing the entire

biosensor temporarily within a sterile chamber. The smaller chamber also reduces the evaporation rate of cell media. Figure 3.2 shows a diagram detailing the changes made to the chamber and the final system design. Figure 3.3 shows a before and after photographs of the CMOS biosensor that is now securely attached to a petri dish.

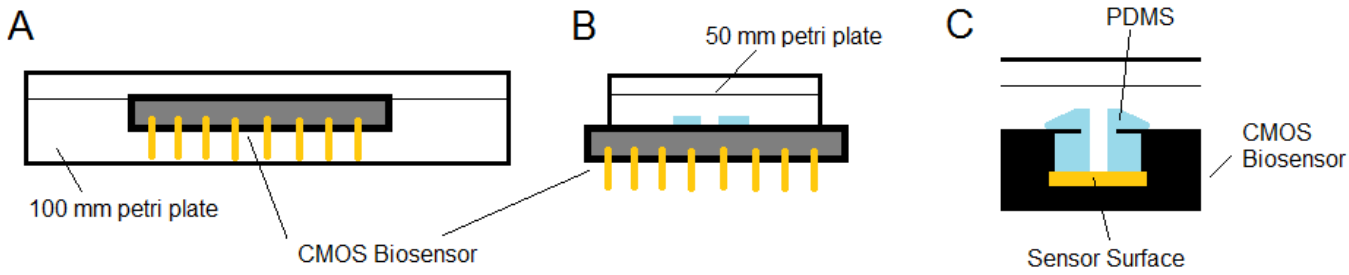

Figure 3.2: This image describes the design of the modified biosensor microfluidic reservoir. Top image A) is the original setup, B) is the modified setup, and C) is a close up of the modifications made, specifically the connection between the petri plate and the CMOS biosensor.

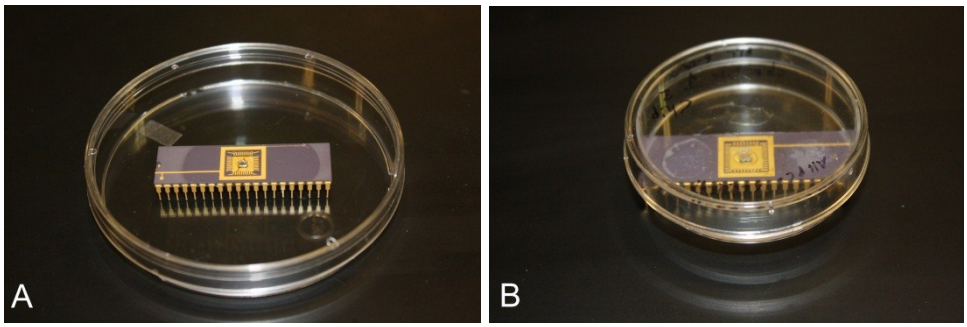

Figure 3.3: Image A shows the CMOS biosensor in the original 100 mm petri plate, and image B shows the modified design.

3.2.3 Surface Treatment of CMOS Biosensor for on-chip Cell Culture

The surface of the CMOS biosensor is silicon oxide, which is non-toxic to AHPCs but not sufficient to support a viable cell culture. To create a viable cell culturing substrate, we chose to test two different surface treatment solutions: cell attachment matrix ECL (ECL) and poly-L-lysine (PLL). ECL and PLL were chosen for this study based on a literature review of devices that supported similar neural cultures [2, 3-4].

To chemically treat the CMOS biosensor chip with ECL, the chip is cleaned by washing with water for 1 hour, rinsing in a 70% ethanol bath, rinsing in deionized water, and finally leaving it under ultraviolet (UV) light for 1 hour. Once the chip is sterile, 0.01% ECL is added to the biosensor surface and left for 24 hours at 5 degrees C. The ECL is then aspirated off and DM is added to culture the cells. Cells are then added on the chip and incubated until imaging.

The preparation for the poly-L-lysine coated biosensors follows a similar method as that of the ECL devices. The devices are first sterilized by washing with water for 1 hour, then rinsed in a 70% ethanol bath, followed by a rinse in deionized water, and finally left under UV for 1 hour. The sterilized devices are coated with 10 µl of PLL for 1 hour. After an hour, the PLL is aspirated off and the device is washed with HBSS 5 times. Once washed, 13ug/ml laminin is added to each of the devices and incubated for 1 hour. Later, the devices are placed in a refrigerator at 5 degrees C overnight (12 hours). The laminin solution is aspirated off the next day and DM solution is added to each of the devices before plating AHPC's onto the surface of the biosensor.

3.2.4 On-chip Cell Culture and Imaging

For this study, rat adult hippocampal progenitor cells (AHPC) were used as the primary neural cell culture. AHPCs were selected because of their pluripotent properties, ease of culturing, and the wealth of literature related to its functioning. AHPCs are pluripotent cells. These cells can differentiate into a wide range of neuronal cells and even into additional AHPCs if there is no differentiation factor present. This allows for research on neural cell differentiation as well as an examination of different cell types produced by the differentiation of AHPCs. Additionally, the same AHPC culture can be used repeatedly for successive experiments, thus reducing the variation between trials. AHPCs are also a robust neural cell type and can survive in conditions too harsh for other cell types such as neurons. This robustness of AHPCs is particularly useful in our studies where the chip and microfluidic designs are continuously being changed.

During our experiments, a culture of AHPC is always maintained for future experiments and also as a control. This colony is cultured in T-25 flasks coated with polyornithine and laminin; flask coating is performed in same manner as for biosensors coated with poly-L-lysine except polyornithine is used in place of poly-L-lysine. The colony is maintained with maintenance media and passed every 3 to 4 days after plating, at approximately 80% confluence. To pass

the maintenance media in the culture flasks, cells are washed with EBSS. The EBSS is then aspirated off and 0.66 ml of tripsin EDTA is added to the flasks to detach the cells from the flask. The flask is then placed within an incubator (37 degree C) for 2 minutes and cells are suspended with 1.7 ml of DMEM/F12. This cell suspension is then centrifuged at 800 RPM for 5 minutes. All media is removed, leaving only a cell pellet which is re-suspended in 100 µl to 400 µl maintenance media depending on size of pellet. The newly re-suspended cells are then used for passing or plated into microfluidic devices.

Devices are imaged at 6, 24, 48, and 72 hours after AHPCs have been plated onto the CMOS biosensor surface. The devices are imaged using a fluorescence microscope (Nikon Microphoto FXA; Nikon, Melville, NY, USA) equipped with a Retiga 2000R digital camera using QCapture software (QImaging, Surrey, BC, Canada). In the case where no cells are present on the chip surface, the chip is cleaned, sterilized, and discontinued from future imaging.

3.2.4 Electronic Readout System

The construction of the electronic readout system is performed in three sections: control unit, control program, and interface circuitry.

The **control unit** is the component that generates and analyzes electric signals. We chose the National Instruments USB 6009 as our control unit. The USB 6009 has sample rate of 48 Ks/s, 8 analog input ports (0 - 10 v), 2 analog output ports (0 - 5 v) and 10 digital input output ports (0/5 v) with independent control for each port. Powered and controlled through a USB cable, the USB 6009 provides a portable analysis system that can be run from a compatible laptop. This feature makes the system portable and ideal for on-site or field-based research. The USB 6009 also provides an all-in-one solution to the analysis of the biosensor chip, especially for repeated testing an array of devices. In addition to portability and functionality, the USB 6009 is fully enclosed, allowing for sterilization and introduction into a cell incubation environment. This is an enviable advantage of USB 6009 over the previously used HP 4145 instrument.

To operate the National Instruments USB 6009, a control program was written in LabView. Controlling the USB 6009, the **control program** simultaneously generates signals, reads signals from the CMOS biosensor transistors, and displays readout values to the user. Due to the large number of FET sensing regions on the biosensor, the USB 6009 uses a two stage

selection system to read signals from the biosensor. The first selection stage is for quadrant selection, which selects what quarter of the device to read from. This is performed by sending selection signals to multiplexers in the interface circuitry. The second selection stage is for individual FET selection, where a single device is selected from an array of FETs. This is performed by activating the gate voltage for a row in the array and the drain voltage for a column; thus activating and selecting a single FET to read from in the array. Column and row excitation is performed directly from the USB 6009 using the analog and digital output ports. To accelerate biosensor analysis, multiple columns (up to 8) can be activated and read at once. Figures A.1 and A.2, in the appendix, show the GUI frontend and the logical block diagram of the control program respectively.

Current values from the biosensor are converted to voltages by the **interface circuitry** and read by USB 6009. Once read, the voltage values are converted back to current values based on constant element values used in the interface circuitry. To convert the current of the biosensor's FET to a corresponding voltage, an array of resistors is used. The design of the conversion circuit for a single FET is shown in Figure 3.3. The current passing through the FET is obtained by measuring the voltage across resistor R1 and dividing by the resistor value for R1 (1 kOhm).

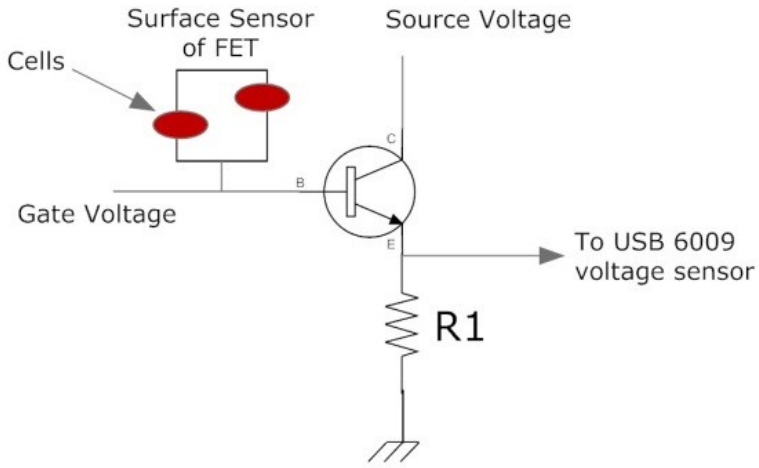

Figure 3.4: Circuit diagram for single current to voltage converter of the interface circuitry.

The chip is designed to have four independent arrays of FETs. To choose any one of the four arrays, quadrant selection is used. Quadrant selection is implemented using 4-to-1 multiplexers [07DGPEK CD4052BE] for each of the 8 analog input ports of the NI USB 6009. The 4 inputs of each multiplexer come from a different quadrant on the biosensor chip and the output is directly

wired to the NI USB 6009. The control signals for all multiplexers are shared and are connected to digital output ports on the NI USB 6009. A complete diagram of the interface circuitry is shown in Figure 3.4 and photo of the completed circuit is shown in Figure 3.5.

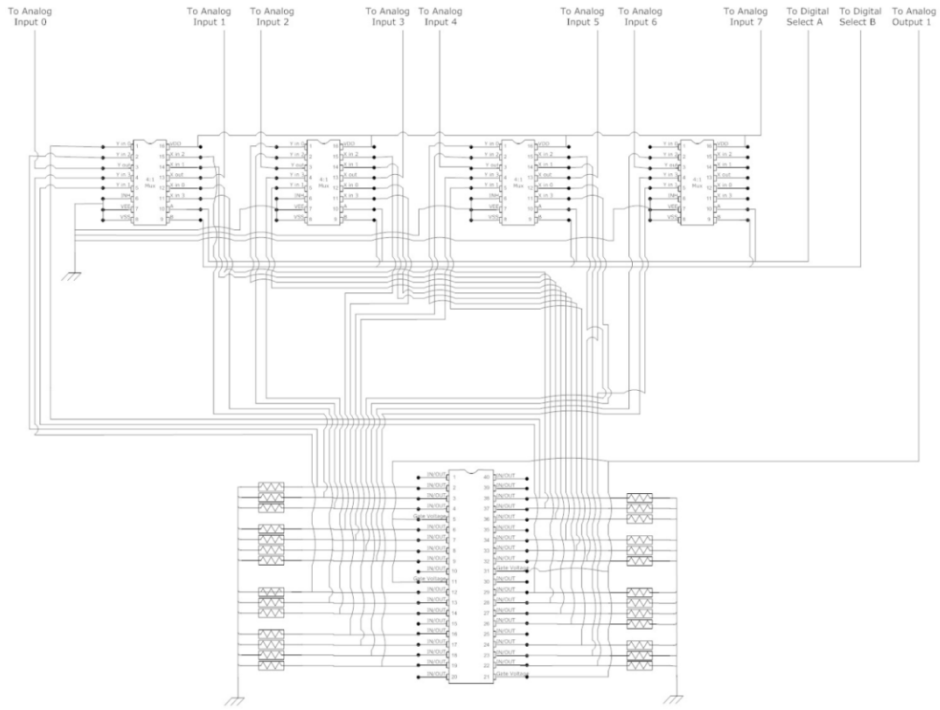

Figure 3.5: Circuit diagram for interface circuitry. Leads at top of the diagram correspond to ports on the National Instruments USB 6009.

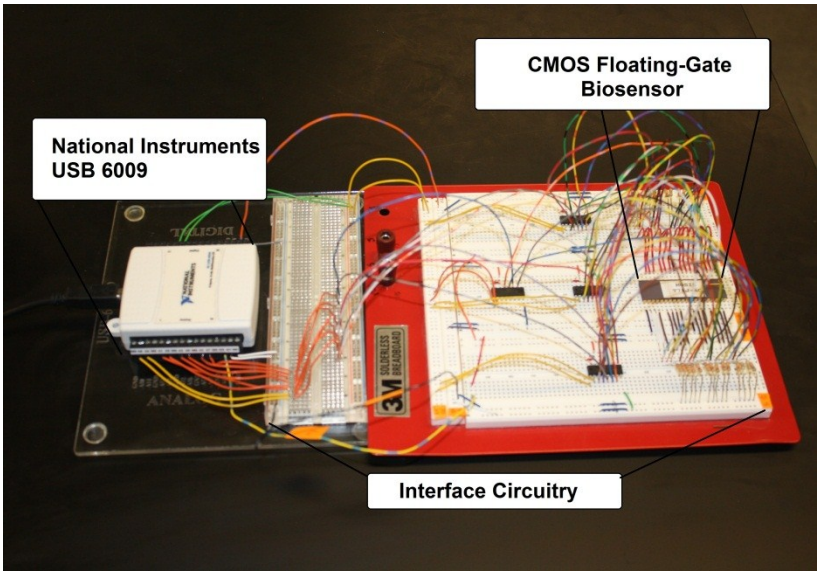

Figure 3.6: Photograph of prototype implementation of the electronic readout system.

3.3 Results

3.3.1 Evaluation of Electronic Readout System

Initial tests on the electronic readout system were performed on individual, commercially-available MOSFET devices [PART#: CD4007UB]. By wiring the USB 6009 directly to the MOSFETs and running the electronic readout system, we observed the current through MOSFETs as shown in Figure 3.6. The screenshot shows the electronic readout system after an analysis of a set of NMOS and PMOS MOSFETS of the control chips [PART#: CD4007UB].

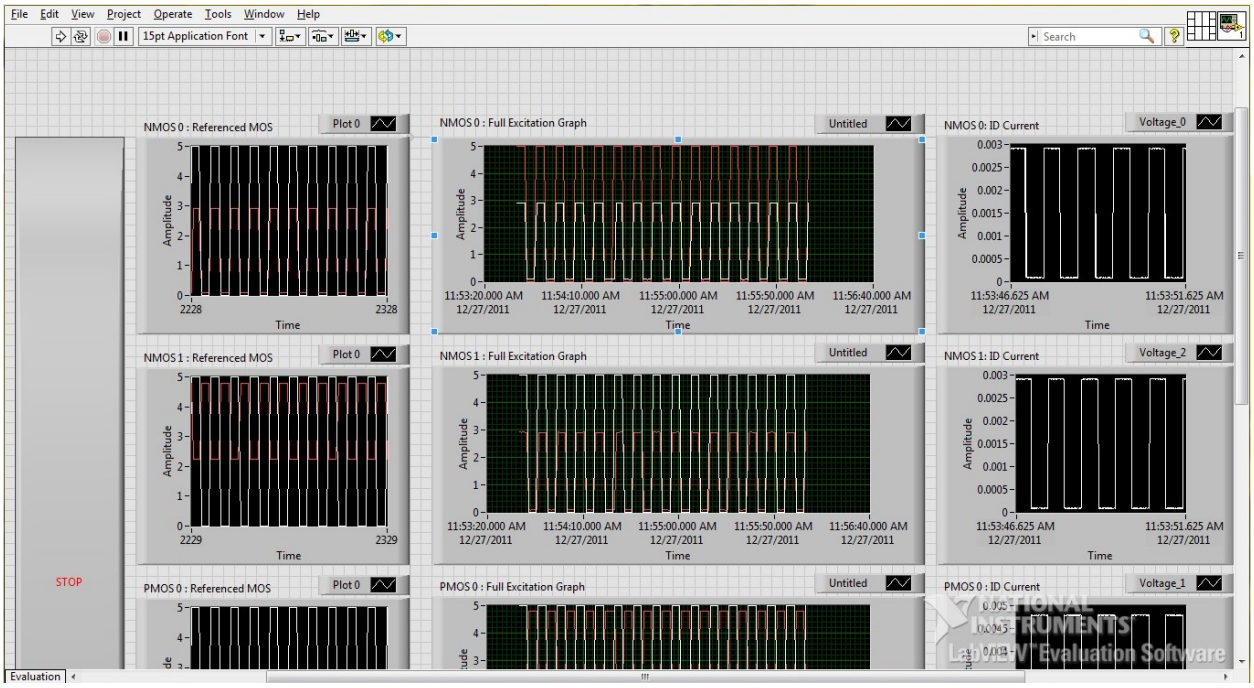

Figure 3.7: This snapshot of the running version of the electronic readout system shows the user interface after a test. The right panels show the input and recorded response voltage at run-time. The middle panel shows the input and recorded response for the entire duration of the test. The right panel shows the current calculated from the observed voltage and the constant resistor values (1 KOhm).

Further testing of the electronic readout system was performed using a test CMOS floating-gate biosensor designed by our group. The test biosensor consisted of 27 FETs and no FET arrays. Several FETs were of different dimensions and were used to check the robustness of our electronic readout system. The analysis of the test biosensor was performed by sweeping the gate voltage from 0 to 5 volts for all the FETs in the biosensor chip. We observed that the FETs

produced current values that roughly matched the expected range and plotted the desired IV curves, confirming the ability of the electronic readout system to analyze a CMOS biosensor.

The quadrant selection functions were tested by implementing a manual channel selection in the program interface, see Figure A.2 in appendix, and running the electronic readout system with several output channels of the biosensor disabled, open circuit, in each quadrant. However, while selecting different regions of the CMOS biosensor, we noticed that certain channels produced no signals, indicating an open circuit or broken bonding wires. We also tested another batch of CMOS floating-gate biosensor, equipped with individual sensing FETs and sensing FET arrays. We noticed that most of the array devices were not functioning. This may be due to the repeated tests we performed on them or some corroded on-chip electrodes. Still we were able to successfully test the basic operations of the electronic readout system for future chips that we plan to get fabricated.

3.3.2 Cell Growth and Viability on CMOS Floating-gate Substrates

In developing a system to analyze neural cells, we examined chemical treatments applied to the biosensor chip surfaces to create a sustainable and viable environment for neural cell cultures. Specifically we examined two surface treatments, poly-L-lysine (PLL) and ECL, and evaluated their effectiveness in promoting cell adhesion and growth by measuring two parameters: duration of surviving cells on surfaces and number of healthy cells in the surviving cultures.

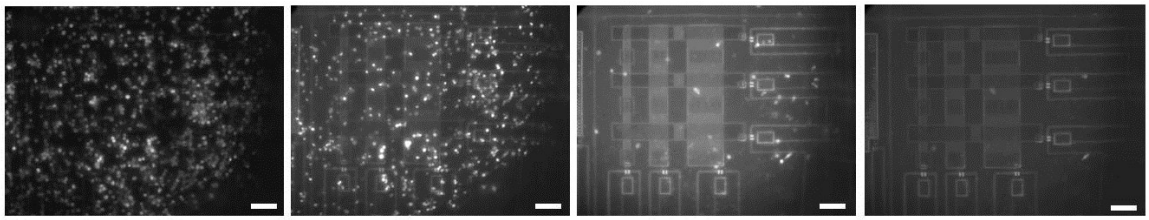

Figure 3.8: Progression of a cell culture over 96 hours after plating. Each image in the sequence is taken 24 hours at 24, 48, 72, and 96 hours for each image respectively. Scale bar is 100 μm.

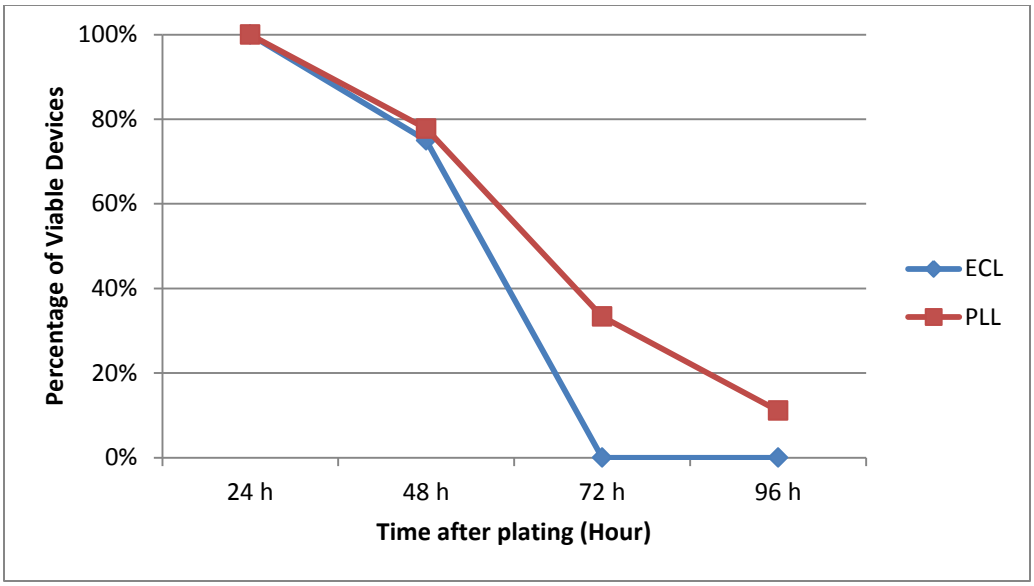

Figure 3.9: Graph of the percentage of viable (cell sustaining) CMOS biosensors versus the time after plating for the surface treatments ECL and PLL.

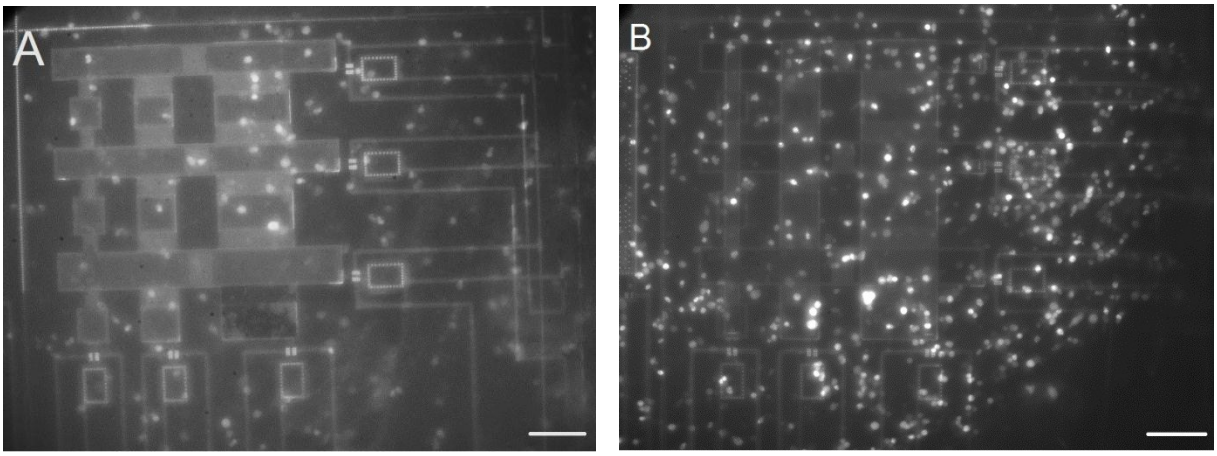

Figure 3.10: Images taken with florescent microscope, cells expressing GPF appear bright. The image on the right shows a culture of AHPC cells on the ECL coated CMOS floating-gate substrate, 48 hours after plating (The contrast of this image was increased by 40% and brightness decreased by 20% to enhance cell visibility). The image on the right is of the same region on the CMOS floating-gate substrate coated with PLL, 48 hours after plating. Scale bar is 100 μm.

As shown in Figure 3.8, the poly-L-lysine coated biosensor chip supported healthy cell cultures for up to 96 hours after plating. The ECL coating supported the cell culture for 48 hours after plating. Further, we observed that cells on poly-L-lysine coated biosensors had more projections than their ECL coated analogs. This is an important metric in determining cell health, as projections represent how well the cells adhere to the surface and make physical/chemical connections with neighboring cells.

3.4 Discussion

In this chapter, we discussed the development of an electronic platform for culturing cells and recording their migration as a function of time. Such an electronic system could negate the use of any time-lapsed microscopy for cell imaging and provide a cheaper alternative to automated stages for such applications. We developed a microscale fluidic reservoir to isolate and encapsulate cell cultures on chip and tested two surface treatment options for long-term cell growth on electronic substrates. We found that poly-L-lysine and laminin are much better for the growth of AHPCs, compared to ECL coatings. We also built a portable electronic readout system to read multiple FET devices in an array using a LabView-controlled National Instrument USB 6009 instrument. Testing with individual transistors shows the proper functioning of this electronic readout system. Upon fabrication of new floating-gate biosensor chips, we will be able to fully test and build upon the first prototype of the electronic readout system.

3.5 Reference

[1] Chen, B. Parashar, A. and Pandey, S. “Folded Floating-Gate CMOS Biosensor for the Detection of Charged Biochemical Molecules,” IEEE Sensors Journal. vol. 11, no 11, pp. 2906-2911. (2011).

[2] Schoen, I., Fromherz, P., " Extracellular stimulation of mammalian neurons through repetitive activation of Na+ channels by weak capacitive currents on a silicon chip,” *Journal of Neurophysiology*, 100(1), pp. 346-57. (2008).

[3] Shinwar, M., Deen, M., and Landheer, D., “Study of the electrolyte-insulator- semiconductor field-effect transistor (EISFET) with applications in biosensor design,” *Microelectron. Reliab*, vol. 47, pp. 2025–2057. (2007).

[4] Hutzler, M., Lambacher, A., Eversmann, B., Jenkner, M., Thewes R., and Fromherz, P., “High-resolution multi-transistor array recording of electrical field potentials in cultured brain slices,” *Journal of Neurophysiology*, 96, pp. 1638-1645. (2006).

[5] Fromherz, P., "Electronic and ionic devices: Semiconductor chips with brain tissue," *Electron Devices Meeting, 2008. IEDM 2008. IEEE International,* pp.1-8, 15-17. (2008).

[6] Schoning, M.J., and A. Poghossian, “BioFEDs (Field-effect devices): State-of-the-art and new directions,” *Electroanalysis*, vol. 19, pp. 1893–1900. (2006).

[7] Chen, L., Topinka, M., LeRoy, M., Westervelt, R., Maranowski, K., and Gossard, A., "Charge-imaging field-effect transistor," *Appl. Phys. Lett.*, vol. 79, no. 8. (2001).

[8] Meyburg, S., Goryll, M., Moers, J., Ingebrandt, S., Bocker-Meffert, S., Luth, H., and Offenhausser, A., "N-Channel field-effect transistors with floating gates for extracellular recordings," *Biosens. Bioelectron.* vol. 21, pp. 1037–1044. (2006).

[9] T. Tokuda, A. Yamamoto, K. Kagawa, M. Nunoshita, and J. Ohta, "A CMOS image sensor with optical and potential dual imaging function for on-chip bioscientific applications," *Sens. Actuators A*, vol. 125, pp. 273–280. (2006).

[10] Kim, D.S., Park, J.E., Shin, J.K., Kim, P., Lim, G., and Park, S.S., "An extended gate FET-based biosensor integrated with a Si microfluidic channel for detection of protein complexes," *Sens. Actuators B*, vol. 117, pp. 488–494. (2006).

Chapter 4

Development of Microfluidic Filter Devices for Neuronal Cell Culture and Migration Studies

4.1 Introduction

4.1.1 Background

In the past decade, several techniques have been developed for observing brain functioning and neural cell signaling. Studies on rat brain, for example, have revealed interesting insights into how the brain responds to a range of stimuli - from injuries, drugs, and even diseases whether any combination of these stimuli can be employed to treat known neurological illnesses. To this end, we present microfluidic filter devices to culture neuronal cells on glass plates to study cell functions such as cell migration and cell signaling in co-culture populations. The use of microfluidics, compared to traditional petri dishes, for cellular studies comes with several key advantages including low reagent volumes, higher throughput, better resolution, and scope of fluid encapsulation.

We plan to follow the in vitro cell culture technique that has been widely used by researchers and has standard protocols that are well published in the literature. In vivo testing, even though

being closer to the real scenario, poses challenges during experimentation and later analysis. Besides, in vivo studies must be ethically justifiable (thus making exploratory studies difficult), are far more expensive, and are limited by lack of real-time analysis of the cellular system. As such, we chose to follow the in vitro cell culture approach that allowed us to testing multiple experimental conditions on different cell populations. Specifically, our microfluidic devices are designed to allow the user to apply/change any media, promote reliable cell adhesion, and even retrieve the cells after growth period. The filter stripes help us to dissociate the physical factors from the chemical factors that affect cell signaling. The development of such co-cultures, especially with different cell types, can ultimately be useful in constructing artificial tissues and organs using the patient's own stem cells.

4.1.2 Objective

The goal of this study is to investigate the migration characteristics of rat adult hippocampal progenitor cells (AHPC) AHPCs in microfluidic filter devices. Working closely with a Neurology lab (Dr. Donald Sakaguchi, ISU), we are designing and testing microfluidic devices to analyze cell migration and co-culture conditions for AHPCs and some other neural cell types.

4.2 Methods and Procedures

4.2.1 Cell Migration and Co-Culture Microfluidic Device Fabrication

The fabrication of the cell migration and co-culture microfluidic devices is performed using similar approach described before in section 2.1.2. The mask layers are designed in AutoCAD for the individual feature layers and additional alignment features are added. The SU-8 fabrication is performed in two phases: first for the 5 µm thick layer and then repeated for the 100 µm thick later. The fabrication of the 5 µm and 100 µm layers are performed using a different SU-8 (SU-8 2005 and SU-8 75 respectively) and adjusted spin speeds.

The co-culture microfluidic device used in this study is composed of three open top 6 mm diameter wells interconnected by 10 µm wide x 5 µm tall channels that are spaced apart by 50 um; each well connects to other two in a triangular formation. In contrast, the migration

microfluidic device consists of two cell culture chambers (100 µm tall x 300 µm wide x 6000 µm long channels) interconnected by 10 µm wide x 5 um tall channels spaced apart by 50 um along the length of the culture chambers. The end of each culture chamber is connected to an 8 mm diameter open top well; creating 4 wells for each device. For both devices, the length of interconnecting channels varies from 100 µm to 1000 µm by 100 µm increments. Photographs of the fabricated co-culture and migration devices are shown in Figure 4.1.

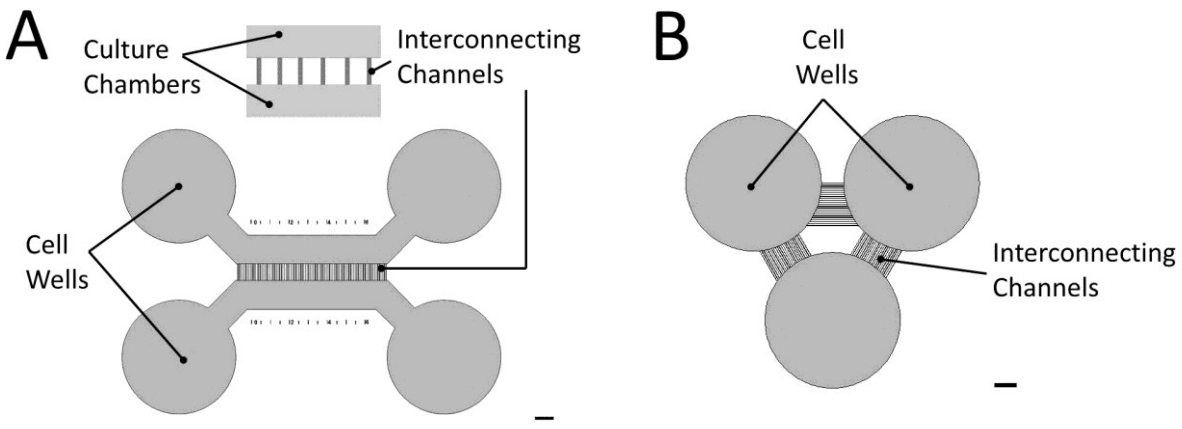

Figure 4.1: Designs of the A) cell migration device and B) co-culture device. Scale bar is 1 mm.

Once the master mold is fabricated, PDMS is poured and bonded to glass slides in the similar manner as previously mentioned. Each device is rinsed in DI water and autoclaved to sterilize the substrates. The devices are coated with an extracellular matrix surface treatment. For this study, two surface treatments are used polyornithine & laminin and ECL. The application of the two surface treatments follows the same steps we used in Chapter 3 to coat the biosensor chip, except that polyornithine is used in place of poly-L-lysine.

Once the devices are coated with either polyornithine & laminin or ECL, AHPC's and other cell types are plated onto them. The GFP expressing AHPCs used in this study belong to the same line as those used in the previous CMOS biosensor study discussed in section 3. The non-GFP expressing AHPCs used were donated by Dr. F. Gage (Salk Institute for Biological Studies, La Jolla, CA. All media in the channels is aspirated off, followed by a rinse with base cell culture media, and then a fill with cell culture maintenance media. Devices are then placed into an incubation chamber for 20 minutes to warm the media before adding the cells. Cells are taken from culture flasks and suspended in maintenance media as described in section 2.2.2. Varying amounts of cell suspensions, between 1 µl and 10 µl, are added to the device cell wells.

Maintenance media is then added on top of the cell wells to create a meniscus of media to prevent dry-out. Devices are then placed within the incubator to culture.

4.2.2 Culturing and Live Imaging

Plated co-culture and migration study chips are kept within an incubator (Temperature = 37 degrees C, CO_2 concentration = 5%). Every 24 hours, the devices are removed from the incubator for imaging and renewal of the cell media. To renew media new maintenance media, differentiation media or drug solution is added to the wells. The exact media added to the well depends on specific experiment being performed. The accompanying container of water is also checked to ensure that an adequate amount of sacrificial water is present (at least 1 ml) to prevent evaporation of the cell media. Live imaging is performed every 24 hours after plating AHPCs on the devices using a microscope equipped with QCapture software (QImaging, Surrey, BC, Canada). Devices are imaged at 40x and 100x in each cell well and regions of interest. Images are saved for analysis.

4.2.3 Fixing and Florescent Imagining

After being plated for at least 72 hours, the cells are fixed, stained, and imaged. The media is removed from all the device wells and washed with a chilled PO_4 buffer before adding paraformaldehyde fixative. The fixative is left in the device wells for 30 minutes before being rinsed and replaced with chilled PO4 buffer. The devices are stained with a 1/50 dapi and 1/200 rhodamine phalloidin staining solution in 0.1 M PO_4 buffer solution for 30 minutes, followed by a rinse of PO_4 buffer solution. Prepared co-culture and cell migration devices are imaged using a fluorescence microscope (Nikon Microphoto FXA; Nikon, Melville, NY, USA) equipped with a Retiga 2000R digital camera and QCapture software (QImaging, Surrey, BC, Canada). When a device is being imaged, a glass slide is placed over the cell wells and the device is flipped to view through the glass slide. If the device is to be imaged with the 100X oil-immersion lens, then after the fixative is removed and washed away with PO_4 buffer before mounting media is placed into the wells. Once the mounting media is placed into all the wells a glass slide is placed over the wells and the device is flipped to image through the glass coverslip.

4.3 Results

4.3.1 Viability Study

In the development of a robust in vitro testing environment, the initial sets of experiments were aimed at culturing healthy neural cells. For this purpose, we plated AHPCs on devices with different surface treatments (polyornithine and ECL) and observing the health and growth of the cultures over time.

In this experiment 13 devices were plated with AHPCs and allowed to culture for 7 days (168 hours after plating). Every 24 hours after plating, the cells were imaged to survey the health of the cells and growth characteristics. The viability of the cells was determined by looking at the following parameters: cultures with surviving cells, cultures with cell projections, and cultures with migrating cells.

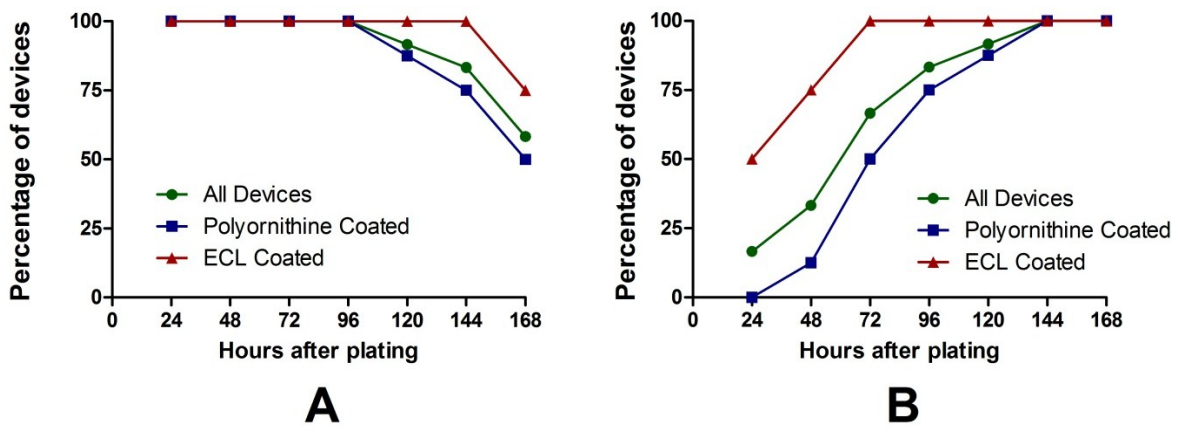

Figure 4.2: Graph "Percentage of Devices with Cell projections" describes the percentage of devices that had cell with healthy cell projections present on the device. Graph "Percentage of Devices with Clustering Cells" describes the percentage of devices that showed cell clustering, the forming of neural spheres. 12 devices were analyzed for this data out of original 13; one ECL coated device became infected at 48 hours and was removed from the study.

For all devices, cell cultures survived the full period of 168 hours (1 week), but 96 hours after plating and beyond cultures showed a slow deterioration in health, as expected in a prolonged culture with only maintenance media. As can be seen from Figure 4.2, polyornithine and ECL have similar effectiveness for culturing cells; although polyornithine coated devices lose cell projects earlier than ECL coated devices, and ECL coated devices have cells grouping before

polyornithine coated devices. Overall, the two surface treatments yielded viable cell cultures and showed little difference in number of surviving cells, cell projections, and clustering cells.

Even though both the surface treatments were effective for our microfluidic devices, we chose to continue our work using the polyornithine coating technique rather than ECL coating technique. polyornithine was chosen over ECL because polyornithine coated devices can be frozen and used at a later date (even for weeks or months); whereas ECL coated devices cannot be stored more than a week. This is particularly advantageous while preparing a large number of devices.

In addition to the successful growth and culture of AHPCs in our devices, we observed that some growing cells were able to migrate into the interconnect channels between wells; figure 4.3. This illustrates that our devices also allows cell migration between two chambers, which can be easily viewed in our transparent device setup. By designing channels with suitable dimensions (10 um wide by 5 um tall), we are able to force the cells to migrate in a single file with clear visual distinctions of the cell body and cell projections.

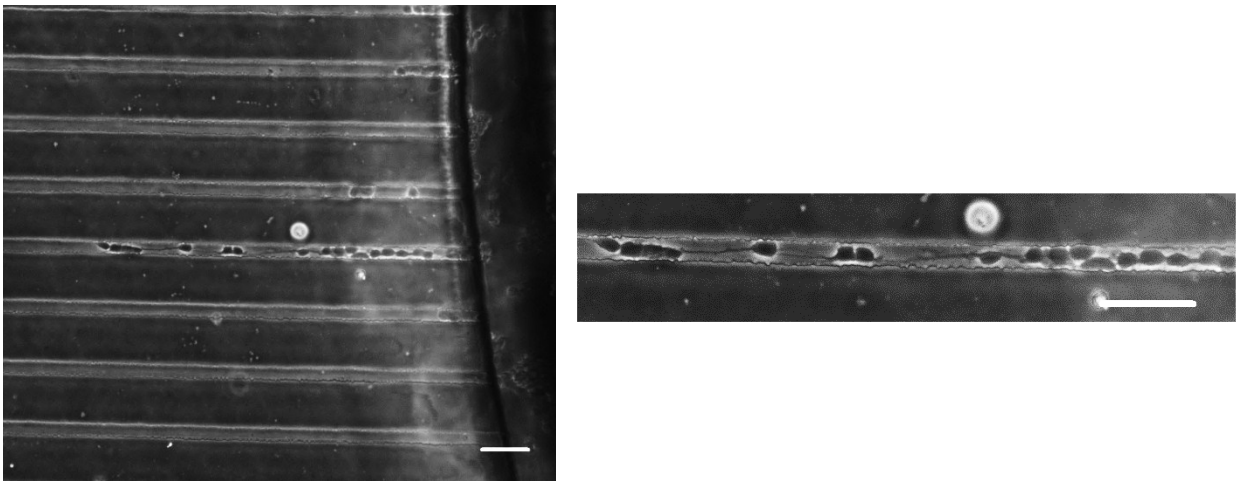

Figure 4.3: AHPCs growing into connecting channels in a co-culture device. To the right is a zoomed view of the central channel shown on the left. Scale bar is 50 μm for both images. Brightness increased by 20% and contrast increased by 40% to enhance cell visibility.

4.3.2 Co-culture Study

After establishing an effective method of surface treating that promotes healthy cell growth, we planned to culture different cell populations in individual interconnected wells (i.e. co-cultures) and study their communication. For the co-culture experiments, 8 devices are coated with polyornithin and laminin surface treatment; 3 co-culture devices and 5 cell migration devices. The devices are prepared and loaded with AHPC GFP expressing cells, AHPC non-GFP expressing cells, and rat RT4 neural cells as described before. For the co-culture devices, all cell types are plated with one cell type per well. The cell migration devices are plated with two cell cultures - one in each chamber with cell pairings of GFP expressing AHPCs with non-GFP expressing AHPCs and GFP expressing AHPCs and RT4 cells. After 72 hours, the cultures are fixed and mounted for subsequent viewing. The images taken over the active growth period are analyzed for any signs of co-culture interaction.

Analyzing the active cell growth images, we found that the AHCP GPF expressing cells showed very low cell counts throughout the experiment. It may be possible that the initial GFP AHPCs cell density was pretty low to develop into a self-sustaining colony. Only a few AHPC GFP expressing cells survived the full 72 hour incubation period. In contrast to the GFP lines, the other two cell types (AHPC non- GFP expressing and RT4 cells) showed healthy growth and network formation. Assuming that all other experimental parameters were the same, this observation supports our hypothesis that the GFP expressing AHPCs failed to growth healthily because they were plated at a low density.

Analyzing the images of fixed cell samples, we found no direct evidence of co-culture interaction. This may be due to the fact that the GFP expressing AHPC cultures were not surviving long enough to interact with the other populations. On a positive note, we did observe that in the healthy cell wells there were a number of cells that approached and entered into the interconnecting channels as shown in figure 4.4. These images also show the high quality of cell imaging possible with the microfluidic devices, as well as the possibility of observing healthy cell growth and interaction across individual wells.

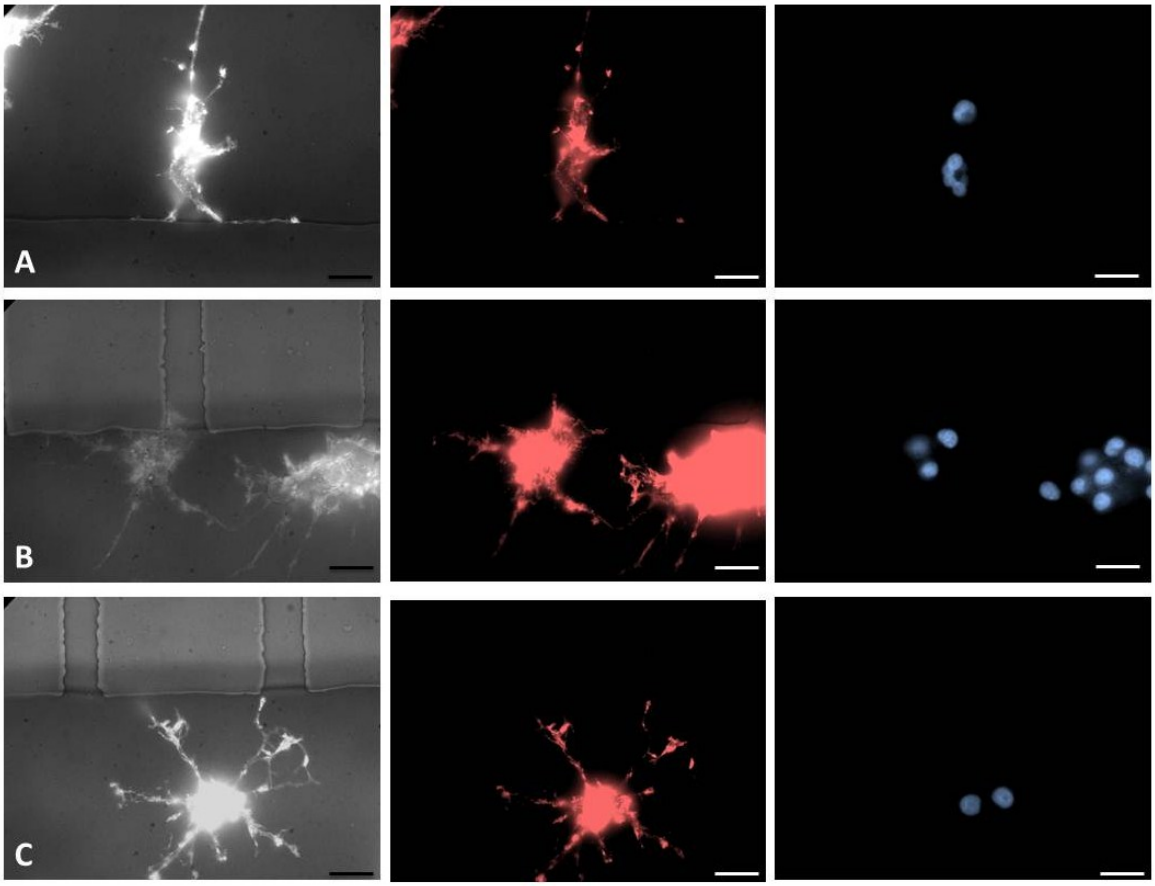

Figure 4.4: Three image series A, B, & C show non-GPF expressing adult rat hippocampal progenitor cells imaged at 600x magnification. Each series of images are comprised of 3 exposures from left to right: light and rhodamine phalloidin fluorescing, rhodamine phalloidin fluorescing, and dapi fluoresce. The first image in series C had its brightness decreased by 20% and contrast increased by 20% to enhance cell projection visibility. Scale bar for all images is 10 μm.

4.4 Discussion

In this chapter, we developed multiple devices for neuronal cell culture based on a microfluidic filter topology. A number of tests were conducted to choose the best surface treatment for cell adhesion in the microfluidic devices. We found that polyorithine and laminin coating works better than ECL coating for neuronal cells. The devices were plated with two or three cell types and their growth was observed for least three days. In some cases, we observed cell projections and cell clustering that indicated a certain level of chemical communication between individual cells. We showed that these cells can be

easily fixed, stained, and imaged with good resolution. Further work is being continued by our group to get reproducible cell growth results in the developed microfluidic filter devices and to develop ways to improve the experimental throughput.

4.5 Reference

[1] Kothapalli, C., Veen, E., Valence, S., Chung, S., Zervantonakis, I., Gertler, F., and Kamm, R., "A high-throughput microfluidic assay to study neurite response togrowth factor gradients," *Lab on a chip*, Issue 3. (2011).

[2] Cheng, S.Y., Heilman, S., Wasserman, M., Archer, S., Shuler, M.L., Wu, M., "A hydrogel-based microfluidic device for the studies of directed cell migration," *Lab on a Chip,* 7(6), pp. 763-9. (2011).

[3] Liu, W.W., Goodhouse, J., Jeon N.L., Enquist, L.W., A Microfluidic Chamber for Analysis of Neuron-to-Cell Spread and Axonal Transport of an Alpha-Herpesvirus. PLoS ONE 3(6): e2382. (2008).

[4] Taylor, A.M., Blurton-Jones, M., Rhee, S.W., Cribbs, D.H., Cotman, C.W., Jeon, N.L., "A microfluidic culture platform for CNS axonal injury, regeneration and transport," *Nature Methods*. 2(8), pp. 599-605. (2005).

[5] Chung, S., Sudo, R., Mack, P.J., Wan, C.R., Vickerman, V., Kamm, R.D., "Cell migration into scaffolds under co-culture conditions in a microfluidic platform," *Lab on a Chip.* 21, 9(2), pp. 269-75. (2009).

[6] Wei, H., Li, H., Mao, S., and Lin, J., "Cell Signaling Analysis by Mass Spectrometry under Co-culture Conditions on an Integrated Microfluidic Device," *Analytical Chemistry, 83* (24), pp. 9306-9313. (2011).

[7] Majumdar, D., Gao, Y., Li, D., Webb, D.J., "Co-culture of neurons and glia in a novel microfluidic platform," Journal of Neuroscience Methods, 196(1), pp. 38-44. (2011).

[8] Millet LJ, Stewart ME, Nuzzo RG, Gillette MU., "Guiding neuron development with planar surface gradients of substrate cues deposited using microfluidic devices," Lab on a Chip, 21, 10(12), pp. 1525-35. (2010)

[9] Taylor, A., Rhee, S., Tu, C., Cribbs, D., Cotman, C., and Jeon, N., "Microfluidic Multicompartment Device for Neuroscience Research," *Langmuir*, *19* (5), pp. 1551–1556. (2003).

[10] Park, J., Kim, S., Li, J., and Han, A., "Quantitative CNS Axon Growth Analysis for Drug Screening in a Microfluidic Neuron Culture Platform" *The 15th International Conference on Miniaturized Systems for Chemistry and Life Sciences (MicroTAS 2011)*, pp. 699-701, Seattle, WA. (2011).

Appendix

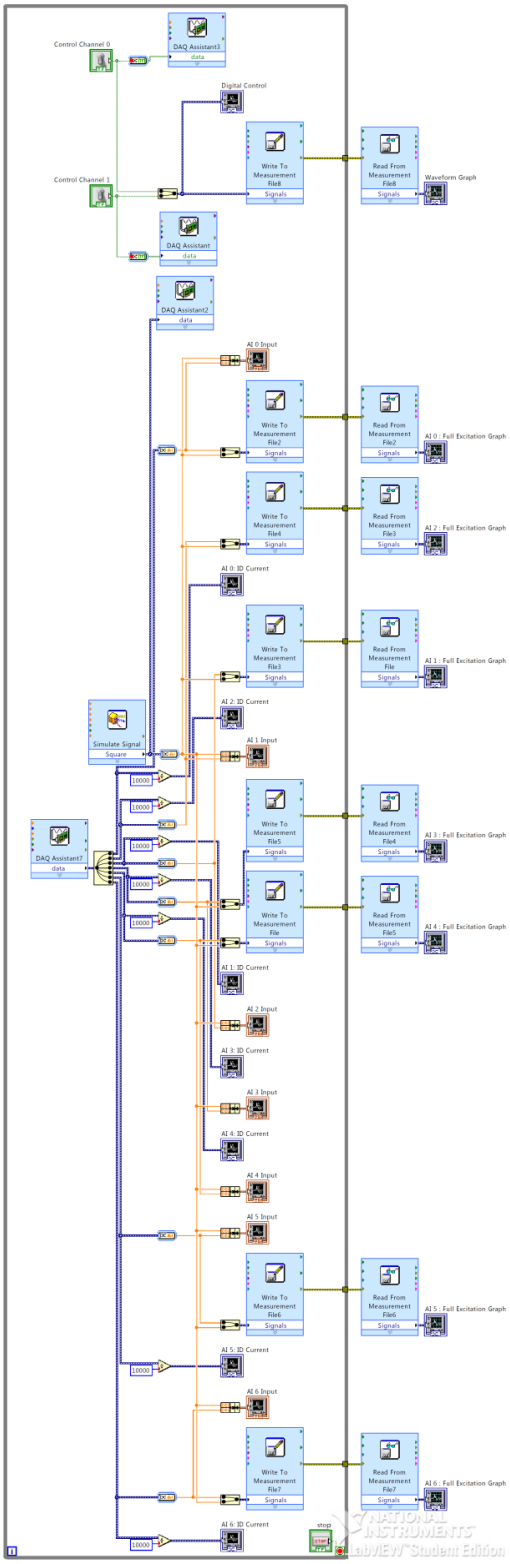

Figure A.1: LabView block diagram code for the control program of the Electronic readout system.